

Cite this: *J. Mater. Chem. A*, 2025, 13, 39557

## Quinones: understanding their electrochemistry, chemistry and degradation pathways to tap their full potential in aqueous redox flow batteries

Afzal,<sup>a</sup> Heshan Liyanaarachchi,<sup>a</sup> Gavin E. Collis,<sup>b</sup> Lathe A. Jones<sup>\*ac</sup> and Subashani Maniam<sup>id</sup><sup>\*a</sup>

Aqueous Organic Redox Flow Batteries (AORFBs) have emerged as a promising alternative for large-scale energy storage. Their advantages include cost-effectiveness due to accessibility of industrial scale quantities of quinone feedstocks, as well as safety and environmental sustainability using aqueous electrolytes. Benzoquinones and related structures such as naphthoquinones and anthraquinones display fascinating chemistry, with biological and redox properties observable in nature, that make them prime candidates for use in AORFBs. A library of quinone-based structures with tuned properties has been studied to this end, however the long-term stability remains a critical challenge, as degradation processes significantly impact the lifetime and overall battery performance. This review is a discussion on the chemistry of quinones including their presence in nature which provides insights into their chemistry, and an analysis of their degradation pathways in AORFBs. Each degradation mechanism contributes to structural decomposition, reducing the amount of redox active material in the RFB system, which presents itself through capacity fade, loss of redox reversibility, and ultimately reducing battery efficiency. Case studies and examples of key degradation pathways are presented to illustrate the main challenges faced in the development of viable AORFBs based on these materials.

Received 17th April 2025  
Accepted 30th September 2025

DOI: 10.1039/d5ta03034j

rsc.li/materials-a

<sup>a</sup>School of Science, STEM College, RMIT University, Melbourne, Victoria, 3001, Australia. E-mail: subashani.maniam@rmit.edu.au<sup>b</sup>CSIRO Manufacturing, CSIRO, Clayton South, Victoria, 3168, Australia. E-mail: gavin.collis@csiro.au<sup>c</sup>Instituto de Síntesis Química y Catálisis Homogénea, Consejo Superior de Investigaciones Científicas (CSIC-ISQCH), CSIC-Universidad de Zaragoza, 50009, Zaragoza, Spain. E-mail: lathe.jones@csic.es

Afzal

Afzal is a chemical engineer with a focus on advanced energy storage technologies. He earned his Master's degree in Chemical Engineering from Dalian University of Technology, China, specializing on hydrocarbon-based polymer membranes for redox flow battery systems with Prof. Dr He Gaohong. Currently he is pursuing a PhD at the RMIT University under the supervision of Dr Subashani Maniam and Assoc. Prof. Lathe

Jones on the development of anolyte active materials based on quinones for aqueous organic redox flow batteries, with an interest in safe, efficient, and sustainable electrochemical energy storage systems.



Heshan Liyanaarachchi

Heshan Liyanaarachchi is an analytical chemist with experience in developing materials for various applications. He obtained his BSc from the University of Kelaniya (Sri Lanka) (2022) in chemistry. He then worked on the World Bank granted AHEAD project as a research fellow at SLIIT (2022–2023) for dye removal in wastewater by using photocatalytic nanomaterials. Currently, he is a Masters by

research student at RMIT University under supervision of Dr Subashani Maniam, Dr Gavin Collis and Dr Tim Jones on materials for non-aqueous redox flow batteries.



# 1 Introduction

The ever increasing market share of renewable energy generated from intermittent sources such as solar<sup>1</sup> and wind and has led to a need for large scale, affordable storage of capacity for later deployment to the grid.<sup>2</sup> Electrochemical energy storage using batteries is a prime candidate,<sup>3</sup> and there are several competing technologies, with Redox Flow Batteries (RFBs) recently attracting significant interest.<sup>4–7</sup> The promise of RFBs is due to the ability to scale capacity based on electrolyte volume, and the option of using benign non-toxic solvents including aqueous solution,<sup>8–11</sup> leading to possible cost and environmental advantages compared to alternative storage technologies such as lithium ion batteries (LIBs). In addition, emerging RFB

technologies have the opportunity to be based on accessible raw materials that can be recycled at end-of-life (EoL).<sup>10</sup>

It is desirable for next generation RFBs to be developed with the circular economy goals in mind. As many countries and their industries transition towards Net Zero Emissions (NZE), considerable effort is being focused on the life cycle of technologies, whereby the chemicals that are used (critical *vs.* sustainable), and the way they are processed and manufactured into products is monitored (*i.e.* energy consumption, waste emissions). In addition, considering the principles of circular economies,<sup>12</sup> how these products and technologies are managed at EoL is a concern, whereby smart material selection can be used to address the 3Rs (reduce, reuse and recycle) therefore minimizing waste and energy, and emission production.<sup>13</sup>

RFBs are composed of redox active couples soluble in a liquid, that can flow between external tanks and the cell stacks (as shown in Fig. 1). A membrane is required to separate the redox pairs in each half-cell, preventing cross-over, and allow passage of ions for charge balance. A specific advantage is the option of employing aqueous electrolytes, which are low in cost and toxicity.<sup>7</sup> Thus, a core focus on RFBs is to provide long duration energy storage beyond LIB technologies.

The development of RFBs has a rich and transformative history, beginning in 1879 with John Doyle's patent for the first zinc–bromine (Zn–Br<sub>2</sub>) flow cell.<sup>14</sup> This early system featured multiple cells but lacked recharge capability, setting a foundation for future innovations. During the late 19th and early 20th centuries, various zinc–halogen battery configurations were explored. In the 1980s, the field experienced a pivotal shift with the development of vanadium redox flow batteries (VRFBs) by researchers at the University of New South Wales (UNSW), led by Maria Skyllas-Kazacos.<sup>15</sup> The introduction of all metal species electrolytes, such as vanadium, capable of operating with two different oxidation states for the catholyte and anolyte respectively, has addressed many of the cross-over issues that



Gavin E. Collis

*Gavin Collis is a Principal Research Scientist at CSIRO, Australia. At the UWA his PhD specialised in the study of novel quinonoid compounds. He held positions as a post-doctoral fellow, Lecturer and Assistant Director of the Nanomaterials Research Centre in Massey University (NZ). At Los Alamos National Laboratory (USA) he contributed to multi-disciplinary projects, being able to commercialize a portable fluorescence*

*detection kit for beryllium. At CSIRO he has been involved in organic electronics, battery recycling, flame-retardant textiles and corrosion inhibitors. His current interest is in developing materials and chemical processes that are sustainable and circular for clean technologies.*



Lathe A. Jones

*Lathe Jones is a Principal Research Scientist (Investigador Científico) at CSIC-ISQCH in Zaragoza, Spain. He obtained his PhD from the University of Queensland (1999) in the area of synthetic coordination chemistry and electrochemistry. He has worked on the electronic properties of ruthenium complexes (University of Manchester, UK), the organometallic chemistry of gold (Zaragoza, Spain), and applied electrochemistry and*

*industrial chemistry (CIDETEC, Spain). From 2010 to 2024 he was an academic at RMIT (Melbourne) specializing in applied electrochemistry and inorganic chemistry, areas in which he maintains an interest, especially with applications in energy.*



Subashani Maniam

*Subashani Maniam is an organic chemist with experience in developing materials for various applications. She obtained her PhD from the ANU (2008) in supramolecular chemistry under the supervision of Prof Christopher Easton. After a joint postdoctoral fellowship at the University of Melbourne and CSIRO (2008–2011) working on dye-sensitised solar cells, she worked at Monash University exploring naphtha-*

*lene diimides- and porphyrin-based photosystems. Currently, she is a Senior Lecturer at RMIT University with interest in materials for redox flow batteries and drug development.*



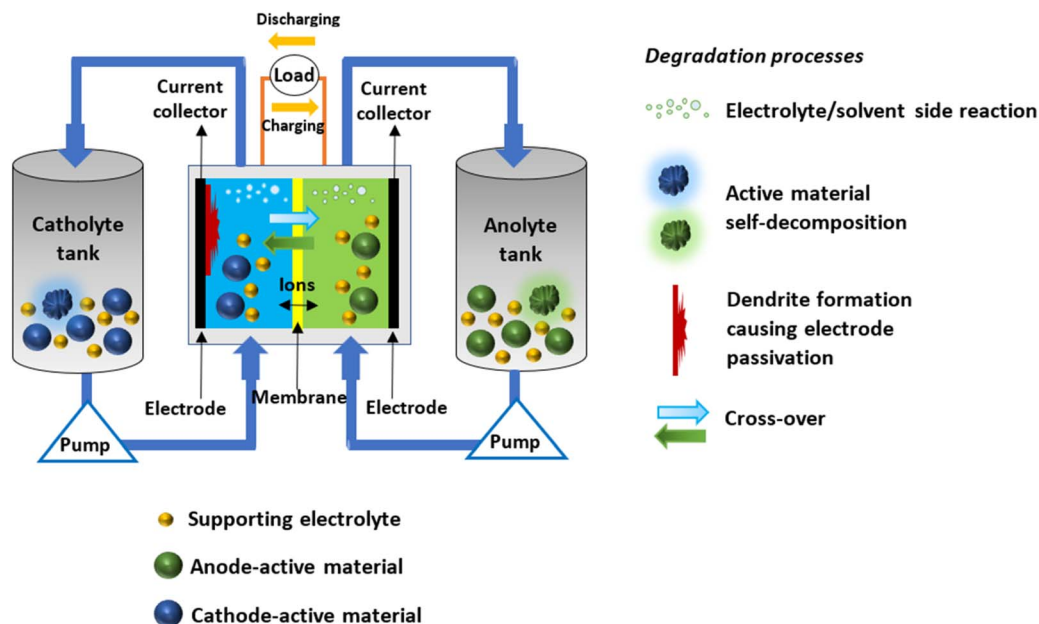


Fig. 1 Schematic representation of a general RFB cell with common degradation mechanisms, including electrolyte and/or solvent side reaction, active material self-decomposition, dendrite formation causing electrode passivation (inorganic RFBs) and cross-over. Adapted with permission,<sup>7</sup> Copyright 2021 Royal Society of Chemistry.

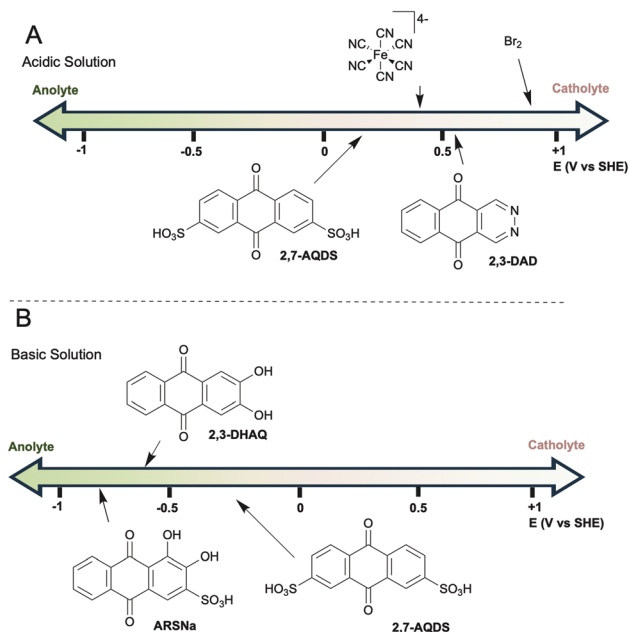
hindered earlier chemistries.<sup>16</sup> The VRFB employs the  $\text{VO}_2^+/\text{VO}_2^+$  and the  $\text{V}^{3+}/\text{V}^{2+}$  redox couples, and allows for independent scaling of energy capacity and power output, making it an attractive solution for large-scale, long-duration energy storage.<sup>17</sup> Other RFB chemistries such as zinc–bromine ( $\text{Zn}-\text{Br}_2$ ), iron–chromium ( $\text{Fe}^{2+}/\text{Fe}^{3+}$ ,  $\text{Cr}^{2+}/\text{Cr}^{3+}$ ), and all-iron ( $\text{Fe}^{2+}/\text{Fe}^{3+}$ ) systems were explored during this period, but each faced unique challenges related to dendrite formation, hydrogen evolution, and limited energy density.<sup>18</sup>

Aqueous organic redox flow batteries (AORFBs) have emerged as a promising alternative to traditional metal-based redox flow batteries, leveraging the tunability of a variety of parameters of organic molecules, inherent safety and scalability of aqueous electrolytes. The interest in quinones as redox-active materials for AORFBs was primarily driven by their favourable redox properties, observable by their presence as redox mediators in natural biological systems, offering high reversibility, tuneable redox potentials, scalability and chemical stability in aqueous solutions.<sup>19</sup>

AORFBs utilize a water soluble organic redox couple on at least one side of the RFB. Compounds such as quinones, which tend to have a relatively negative redox potential, will often be used to formulate the anolyte, with an inorganic couple as the catholyte. However, the synthetic versatility of quinones allows tuning of redox potentials, enabling quinones to be used in the catholyte if the reversible potential is sufficiently positive.

Scheme 1 shows some typical redox potentials on the Standard Hydrogen Electrode (SHE) scale. An AORFB would be constructed by taking two materials, each with a reversible redox process, where the material with the more negative potential will constitute the anolyte, and the more positive potential will be the catholyte, in a cell such as that shown in

Fig. 1. The greater the separation of the two redox processes, the greater the maximum theoretical voltage of the RFB will be. The inorganic couples shown as examples, iron hexacyanide ( $[\text{Fe}(\text{CN})_6]^{3-/4-}$ ) and bromine ( $\text{Br}_2/\text{Br}^-$ ), will act as catholytes,



Scheme 1 Schematic representation of reported redox potentials of some inorganic and organic species used in RFBs. (A) Strongly acidic solution 2,7-AQDS<sup>20,21</sup> and 2,3-DAD<sup>20</sup> and (B) strongly basic solution 2,3-DHAQ,<sup>22</sup> 2,7-AQDS<sup>20</sup> and ARSNa.<sup>23</sup> The examples show schematically how synthetic tuning of quinones changes redox potential and the effect of pH.



allowing cell construction with the more negative quinones as anolytes. Fully organic AORFBs can be designed if the two organic species are separated sufficiently in  $E$  values to attain an acceptable voltage.

Whether a quinone is used as a catholyte or anolyte depends upon the redox potential of the quinone, which is pH dependent, relative to the couple in the other half cell. For example, with  $\text{Br}_2/\text{Br}^-$  as a catholyte, a 2,3-DAD based acid anolyte (Scheme 1A) would give a relatively small cell voltage compared to alternative such as 2,7-AQDS, observable by the difference in  $E$  values in Scheme 1A.<sup>21</sup> The redox potential of the quinone will depend on the presence of electron withdrawing (EWGs) and donating groups (EDGs), the core structure, and the pH at which the RFB operates. As in other systems,<sup>24</sup> the same compound may have very different redox (cell voltage, potential), chemical (stability), optical, biological (activity) and physical (solubility) properties as they are dramatically influenced by pH. The influence of pH can also make it difficult to select possible quinone candidates in the design phase of new materials.<sup>24</sup> For example, note the large difference in  $E$  for 2,7-AQDS in acidic (Scheme 1A) and basic solution (Scheme 1B),<sup>20</sup> separated by approximately 0.54 V, with a more significantly more negative  $E$  in basic solution. The strategy for tuning the redox potential of quinones is thus based upon the balance of solubility with the use of electron withdrawing groups ( $-\text{SO}_3\text{H}$ ,  $-\text{CO}_2\text{R}$ ) which will move  $E$  to more positive values, and the use of electron donating ( $-\text{OH}$ ,  $-\text{NH}_2$ ,  $-\text{R}$ ,  $-\text{Ar}$ ) groups to move the  $E$  value more negative,<sup>25</sup> as well as other synthetic strategies such as the introduction of heteroatoms (*e.g.* N) (*e.g.* 2,3-DAD, Scheme 1A). The use of electron donating groups will lower  $E$  values and lead to higher voltages in the RFB when the quinone is used as a catholyte, to alleviate the relatively low voltage of quinone-bromide RFBs.<sup>21</sup> The introduction of an  $-\text{OH}$  group will invoke a much larger negative shift in basic solution compared to acidic solution if the  $-\text{OH}$  group is deprotonated.<sup>20</sup>

The replacement of carbon atoms in the quinone ring system with heteroatoms is another way to change the properties of the quinone electrolyte. For example, introduction of the diaza moiety in the 2,3 position, such as in 2,3-DAD, leads to a positive shift of approximately 300 mV compared to the 2,7-AQDS structure (Scheme 1A), making such structures useful as catholytes.<sup>20</sup>

Care should also be taken in comparing quinone anolytes in different RFB systems, as other parameters such as concentration, the type of catholyte, membrane used, supporting electrolyte and pH are significantly different especially with acidic functional groups, and simple comparisons should not be made. This could be resolved by the development and use of a standard assay where fixed parameters are used by the RFB community.

The use of a quinone as a catholyte instead of inorganic species is an option in all-organic AORFBs. For example, 2,7-AQDS ( $E^0 \sim +0.20$  V vs. SHE in acid)<sup>26</sup> can be used as a catholyte or an anolyte.

In Scheme 1B representative  $E$  values in strongly basic solution are also shown, with the use of phenolic groups in strong base in compounds such as  $\text{ARSNa}^{23}$  and 2,3-DHAQ<sup>22</sup>

increasing the solubility and moving the  $E$  values negative to achieve higher performance RFBs.

The synthesis of a quinone soluble material for aqueous solutions, design of a cell with two appropriate materials, and membrane for a specific pH and porosity is the starting point for development of a quinone-based AORFB. However, the longevity and subsequent viability of a quinone material will depend on its stability in the electrolyte under redox cycling (between the reduced, neutral and oxidized states), over a long period of time, high solubility, and its resistance to degradation pathways that may occur.

The presence of a variety of quinonoid compounds in nature and industrial applications, with their unique robustness is what ultimately has inspired their use in AORFBs. In this review we will discuss the properties and characteristics of quinones, including their redox and chemical properties in nature and industry, and factors which make them fascinating redox active molecules for use in AORFBs. We will then present a discussion aimed at a broad audience on common degradation mechanisms by using examples and illustrative case studies. It is an understanding of how to prevent or minimize these degradation pathways, combined with the design of molecules that are highly soluble in aqueous solutions, that will enable the full potential of quinones in AORFBs to be realized. The key is the future design of molecules that circumvent loss of capacity due to chemical and electrochemical degradation processes under RFB conditions.

## 2 Quinones: from biology, dyestuff and materials science

Quinones constitute an interesting and important class of organic compounds. They can be considered as a simple cross-conjugated system that possess an alternating pattern of single and double bonds, which includes the exocyclic oxygen atom. The nomenclature of these systems is closely related to polycyclic aromatic hydrocarbons and some common examples are shown in Fig. 2 with their common names and Chemical Abstract names in parentheses.

### 2.1 Electrochemistry and redox properties of quinones

Electron transfer reactions in biological systems rely upon quinones for a variety of physiological processes.<sup>27</sup> It is these natural redox properties of quinones that inspire the application of quinones in AORFBs, as they are evidence for good redox reversibility and fast kinetics that are crucial for applications in energy storage.

An understanding of quinone redox processes is necessary to appreciate their role in AORFBs, leading to an awareness of the stable chemical form of both the reduced, neutral and oxidized species in a RFB couple, and to comprehend the degradation mechanisms that are discussed in this review.

A simplified outline of key redox processes with examples are shown in Scheme 2, which shows the two-electron stepwise reduction of quinone through the semiquinone intermediate



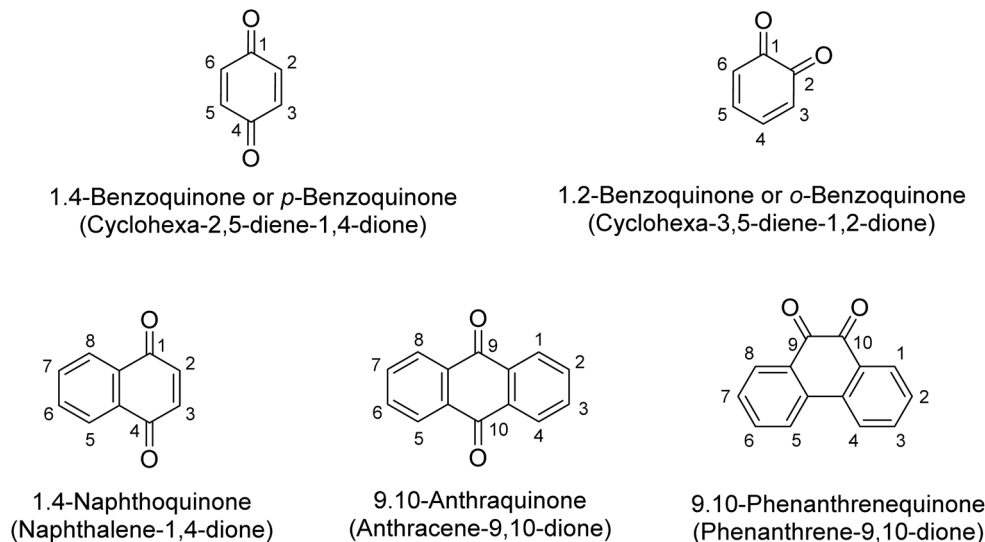
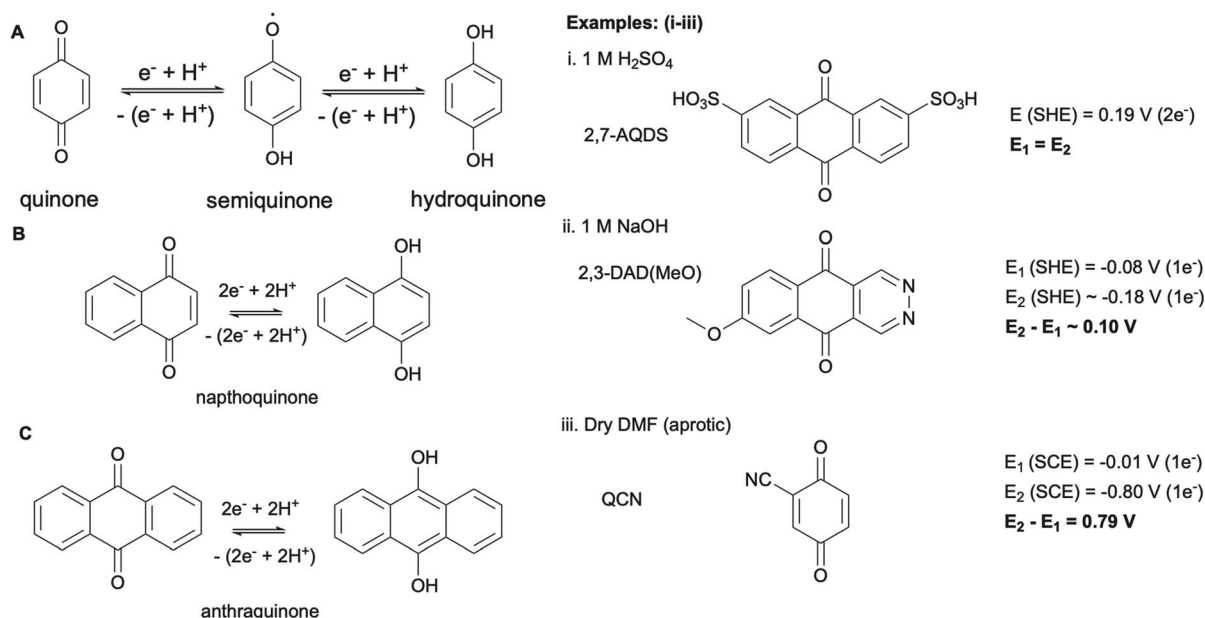


Fig. 2 Structures of quinone with their common and Chemical Abstract names.

Scheme 2 Redox properties of quinones, showing quinone, semiquinone and hydroquinone through successive  $1e^-$  reductions, and the products of two electron reductions of naphthoquinone and anthraquinone. Examples in acid (A)–(C) and (i),<sup>26</sup> base (ii)<sup>20</sup> and organic solution (iii)<sup>27</sup> showing the separation of the two successive reductions in the aprotic solvent.

(A), and also shows the products formed from the two-electron reduction of naphthoquinone (B) and anthraquinone (C).

In the presence of protons (for example in acidic aqueous solution), quinone (Q) is reduced to the hydroquinone (QH<sub>2</sub>) in a process involving two electrons and two protons (Scheme 2A). The two redox potentials  $E_1$  and  $E_2$ , representing the stepwise transfer of each electron through a semiquinone intermediate, tend to be energetically similar in aqueous acidic solutions, as Proton Coupled Electron Transfer (PCET) is taking place, and protonation of the semiquinone intermediate facilitates the second reduction at  $E_2$ .<sup>28</sup> In basic solution, due to the lack of

protons, PCET is hampered and the second reduction may be more difficult, with reduction proceeding to the dianion  $Q^{2-}$  in strongly basic solutions.  $Q^{2-}$  may also be formed at intermediate pH values, depending on the  $pK_a$  of the hydroquinone. For the purpose of this review, redox processes of quinones in aqueous solution in RFBs can thus be considered two-electron processes to QH<sub>2</sub> commonly in strongly acidic solution or  $Q^{2-}$  in strongly basic solution, where sulfuric acid (H<sub>2</sub>SO<sub>4</sub>) or sodium or potassium hydroxide (NaOH or KOH) are the most popular solvents. Redox behaviour at intermediate pH values has been studied and reviewed by other authors, making



detailed aspects of the redox chemistry of quinone available in the literature.<sup>29,30</sup>

In dry aprotic organic solvents, there are no protons present for PCET, and a semiquinone ( $Q^{\cdot-}$ ) radical is formed by a one electron reduction process, followed by formation of the  $Q^{2-}$  dianion after delivery of another electron. This second reduction may have a potential ( $E_2$ ) quite separated from the radical formation ( $E_1$ ) due to the higher stability of the radical in the absence of protons or hydrogen bonding.

Scheme 2 shows three examples (i, ii and iii), with the two successive reduction processes represented as  $E_1$  and  $E_2$ . In 1 M  $H_2SO_4$  (low pH),  $E_1 \approx E_2$  (example i), while in 1 M NaOH (high pH) there is a slight separation of the two electron transfer processes (example ii) in this example 2,3-DAD(MeO). Both acidic and basic solutions have been used for the electrolyte in AORFBs, as seen by examples later in this paper, and the degradation processes are dependent upon the chemical structure of these species and their reactivity at different pH. In aprotic organic solution (Scheme 2, example iii) PCET is not possible, and the hydroxyl functional group cannot be formed, so successive reductions of the  $Q^{\cdot-}$  to  $Q^{2-}$  species are observed that may be quite separated in energy (see  $E_1 - E_2 = 0.79$  V separation in example iii for the cyanoquinone), though experimental design can facilitate transfer of two electrons at similar energies in these systems if required.

The study of these redox processes *via* electrochemical methods such as voltammetry allows the main chemical and electrochemical characteristics of the quinones to be elucidated, leading to an understanding of the redox processes linked to degradation mechanisms. An understanding of the voltammetry of quinones has been described in various papers and reviews,<sup>27,29,30</sup> and the main aspects relevant to this review are the key parameters that give kinetic, reversibility and stability information.<sup>31</sup>

The heterogeneous rate constant for the electron transfer ( $k^0$ ) may be electrochemically determined.<sup>31</sup> An advantage of quinones are that the heterogeneous kinetics are generally fast, often several orders of magnitude higher than inorganic species, and this is observable in the peak separation of reversible voltammograms approaching 59/n mV even at higher voltammetric scan rates.

Initial screening of degradation in a chosen electrolyte is often undertaken *via* voltammetric studies, where the reversibility of the redox process in the electrolyte used is gauged. A loss in peak intensity observed in the cyclic voltammogram return wave due to precipitation or chemical reaction indicates chemical irreversibility due to unwanted degradation processes. Voltammetric cycling of the redox couple in the electrolyte is thus one of the first steps in characterization of a new candidate for AORFBs to identify chemical stability and possible degradation of the reduced, intermediate and oxidized forms of the active species. These voltammetric studies, combined with other electrochemical studies, will also allow determination of the diffusion coefficients ( $D$ ) which is important for mass transport, and the standard redox potential for information about the thermodynamics of the redox process ( $E$ ).<sup>32</sup> Molecular design for AORFBs will target molecules that are chemically reversible

(stable to degradation in both the oxidized, intermediate and reduced forms in the electrolyte), and highly soluble with fast heterogeneous electron transfer kinetics.

Table 1 gives some representative examples of RFB configurations with solubilities, coupled anolyte/catholytes, full cell voltage and some key parameters as an indication of some performance characteristics. Included in Table 1 are vanadium, Zn-halide and some quinone-based RFBs. It should be noted that there are limitations to directly compare these cell configurations as the experimental testing conditions and parameters are not standardized. Inorganic active materials for RFB are limited by the speciation of specific chemical species with defined redox potentials, whereas the advantage of organic-based RFBs is that they can be designed to overcome limitations associated with electrochemical, chemical, biological and physical properties *via* molecular design. High performing RFBs will need redox active species that have solubilities in the molar (M) range (see examples from 0.1 M to several M in Table 1), and be stable under redox cycling from hundreds of cycles in laboratory testing to tens of thousands of cycles in real world systems, with minimal loss in capacity.

The data in Table 1 is a general guide, useful for comparing some properties of quinone based RFBs with other metal-based electrolyte cells. The key is to design quinones with an appropriate redox potential that allows a maximum theoretical cell potential within the limits of the stability of water. Loss of performance under cycling can be due to a range of factors, such as cross contamination across the membrane (cross-over), membrane failure or inadequate for organic redox mediators, precipitation, electrolyte degradation, which been covered in previous reviews by others.<sup>9,11,33–38</sup> The stability of quinones to degradation through aqueous organic reactions is a key focus of this review, as it is a fundamental consideration when designing novel molecules, which we will discuss later in this manuscript. Future implementation would require AORFBs based on quinones to be competitive with vanadium-based RFBs, especially noting the higher cell voltages of the inorganic systems in Table 1.

## 2.2 Biological uses, industrial applications and theoretical studies

Quinones are one of the oldest classes of organic compounds and are known for their association with the dye industry, biochemical processes and early concepts pertaining to bond delocalization and aromaticity. The drive behind this interest is the ease which quinones/hydroquinones can be chemically modified to adjust the chemical, physical, optical, electrochemical and biological properties of the material depending on end-use applications.

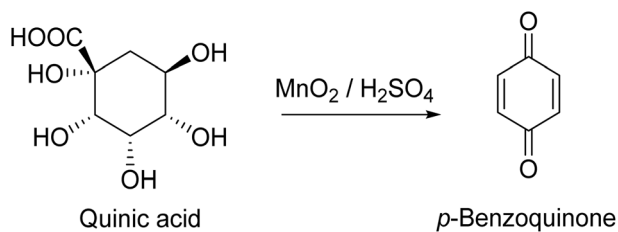
The generic name of quinone originates from the material that was used in the synthesis of the first quinonoid compound, undertaken in Liebig's laboratory in the 1950s, where a sustainable source of a sugar precursor, quinic acid, which when chemically oxidized with manganese dioxide in  $H_2SO_4$ , produced a highly coloured compound, named *p*-benzoquinone.<sup>48</sup> (Scheme 3).



Table 1 Example of neutral, acidic and basic operating RFB systems and the corresponding battery parameters

Anolyte (conc.)	Catholyte (conc.)	Membrane	Cell voltage (V)	Current density (mA cm <sup>-2</sup> )	Cut-off voltage (V)	Coulombic efficiency (%)	Discharge capacity (Ah L <sup>-1</sup> )	Capacity loss rate	Cycle number	Ref.
<b>Neutral</b>										
2,7-AQDS (0.2 M in Na <sub>2</sub> SO <sub>4</sub> )	HQS (0.2 M in Na <sub>2</sub> SO <sub>4</sub> )	Nafion 117	0.90	60	0.0–1.5	96–97	7.6	—	120	39
0.4 M ZnBr <sub>2</sub> (2.0 M KCl)	0.8 M FeCl <sub>2</sub> (1.6 M glycine and 2.0 M KCl)	PBI	1.43	40	0.1–1.75	97–98	40	—	100	40
<b>Acidic</b>										
2,7-AQDS (0.2 M in 1 M H <sub>2</sub> SO <sub>4</sub> )	TSPSQ (0.2 M in 1 M H <sub>2</sub> SO <sub>4</sub> )	Nafion 117	0.41	50	0.0–0.6	99–100	87–88	0.013% per cycle	150	41
2,7-AQDS (0.1 M in 1 M H <sub>2</sub> SO <sub>4</sub> )	1,2-Dihydroxybenzene-3,5-disulfonic acid (0.1 M in 1 M H <sub>2</sub> SO <sub>4</sub> )	Nafion 117	0.3	80	0.005–1.000	n/a	n/a	n/a	30	42
V <sup>2+</sup> /V <sup>3+</sup>	V <sup>4+</sup> /V <sup>5+</sup>	Nafion 115	1.15–1.55	80–200	0.7–1.9	95–99	25–47	0.25% per cycle	12 000–14 000	43 and 44
3 M ZnBr <sub>2</sub> (6 M KI)	I <sub>2</sub>	Polyolefin membrane	1.33	80	Capacity limit	95	30	—	1000	45
<b>Basic</b>										
Lawsonite (0.4 M in 0.8 M KOH/0.2 M K <sub>2</sub> SO <sub>3</sub> )	K <sub>4</sub> [Fe(CN) <sub>6</sub> ] (0.4 M in 1 M KOH)	Nafion 117	1.01	100	0.2–1.6	99	20.27	0.1% per cycle	100	46
0.1 M TSAQ in 1 M NaOH	K <sub>4</sub> [Fe(CN) <sub>6</sub> ]/(0.1 M) and K <sub>3</sub> [Fe(CN) <sub>6</sub> ] (0.02 M) in 1 M NaOH	Nafion 212	1.14	40	0.6–1.4	99.9	4.76	0.025% per day	900	47





Scheme 3 Chemical oxidation of quinic acid to form *p*-benzoquinone.

Due to their strong, bright colours and chemical robustness, naturally occurring quinones from plants and animals have been used as dyes in the colourant industry.<sup>49</sup> The most ancient quinone dye known as Kermes, is extracted from insects (*Kermococcus ilicis*) which infest the kermes oak tree. A number of naturally quinone dyes, such as alizarin<sup>50</sup> and quinizarin,<sup>50</sup> are shown in Fig. 3.

The accidental synthesis of mauveine by Perkins in 1865,<sup>51</sup> opened the way to chemically synthesize quinone compounds and therefore be less reliant on the use of natural dye sources. For example, alizarin could be made using fossil based synthetic feedstocks, such as anthracene, allowing large scale industrial quantities to be accessed easily and cheaply. BASF developed indigo and several other common dyes such as the ones shown in Fig. 3B.<sup>52</sup>

Quinones also play a key role in biological systems due to their unique redox properties and low toxicity to the environment. They are of importance for their medicinal properties, while others are observed to take part in physiological processes. Natural quinones are found in evolved species of bacteria, fungi, plants and to a lesser extent animals. From a biochemical viewpoint, quinones such as co-enzyme Q and vitamin K<sub>1</sub> (Fig. 3C) are vital because of their reduction/oxidation properties. The semiquinone radical generated from vitamin K<sub>1</sub> allows the material to participate as either an electron donor or acceptor at the cellular level.<sup>53</sup> Also, an example of solubility tuning, the presence of the long isoprenoid tail makes

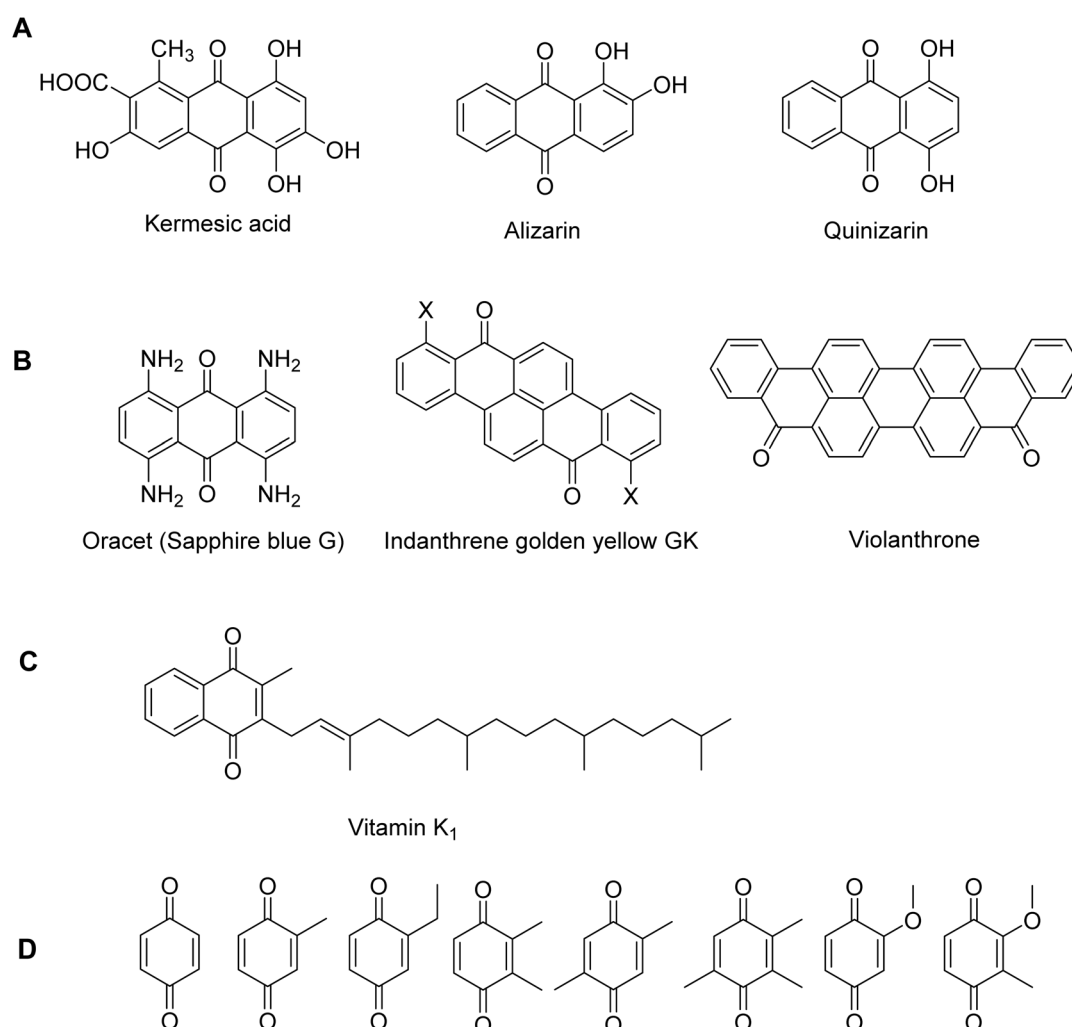


Fig. 3 (A) Some examples of naturally occurring quinone structures. (B) Quinone-based dyes developed by BASF. (C) Structure of vitamin K<sub>1</sub>. (D) Examples of *p*-benzoquinones from arthropods developed as defensive agents.



the structure highly non-polar which enables it to diffuse rapidly the hydrocarbon phase of the mitochondrial membrane.<sup>54</sup>

Likewise, simple *p*-benzoquinones have been identified from arthropods as defensive agents. As shown in Fig. 3D, eight chemical deterrents were obtained from arachnids, millipedes, beetles, earwigs and termites. An example of how the insects uses such chemicals was shown by Eisner and colleagues using remarkable photographic techniques at the time.<sup>55,56</sup> The beetle can be seen discharging a fine spray. Quinols are stocked in the defensive glands; however, the quinols are subjected to hydrogen peroxide under catalytic conditions, whereby quinones are propelled at temperature up to 100 °C as a thermal deterrent.

Many natural quinones are of interest because of their medicinal properties and some interesting examples showing their unique properties are highlighted below.<sup>57,58</sup> Two examples of compounds that have attracted interest has been Dynemicin A and Conocurvone (Fig. 4) isolated from a microorganism and plant extracts, respectively. The former compound has shown antitumor antibiotic activity where the mechanism proposed is unusual and unique, with the quinone being reduced to the hydroquinone causing the acetylenic system to cyclize forming an extremely rare and reactive diradical species that has cytotoxic properties capable of DNA cleavage.

In contrast, Conocurvone<sup>59</sup> is the trimeric form of naturally occurring Teretifolione B, which was isolated from extracts

from the West Australian Smoke Bush. It has shown inhibitory against both HIV integrase and HIV mediated cell fusion, but what is most startlingly is the monomer Teretifolione does not show any activity.

As a result of the unique properties of quinones they have been of interest of advancing the use of fundamental understanding of bond localization (quinone form), aromaticity (hydroquinone form) and materials applications. Fundamental studies of strained fused quinones relating to bond fixation and stability have been undertaken, where some quinones<sup>60</sup> are stable at room temperature whereas others can only be generated at  $-78$  °C and trapped due to the extremely reactive nature of the quinone double bond. Likewise, cyclopropane-fused quinones are found in many biological systems and the synthetic routes used to develop these novel compounds have been applied to access natural products of medicinal interest.<sup>61–63</sup>

The synthetic chemistry of quinone-based materials is extremely flexible; thus, they have been studied in energy generation and storage applications. Our team has shown that a simple and cheap hydroquinone dye, Anthrasol Golden Yellow 1GKE, could be easily converted in two steps to afford a stable, high performing p-type acceptor for bulk heterojunction solar cells.<sup>64</sup> Likewise for energy storage, the bis-sulfate ester of hydroquinones have been studied as possible materials for cathode electrode materials in LIBs or novel electrolytes in RFBs. A classic example is the use of a calixarene quinone as a replacement for metal rich cathode materials reported in 2013

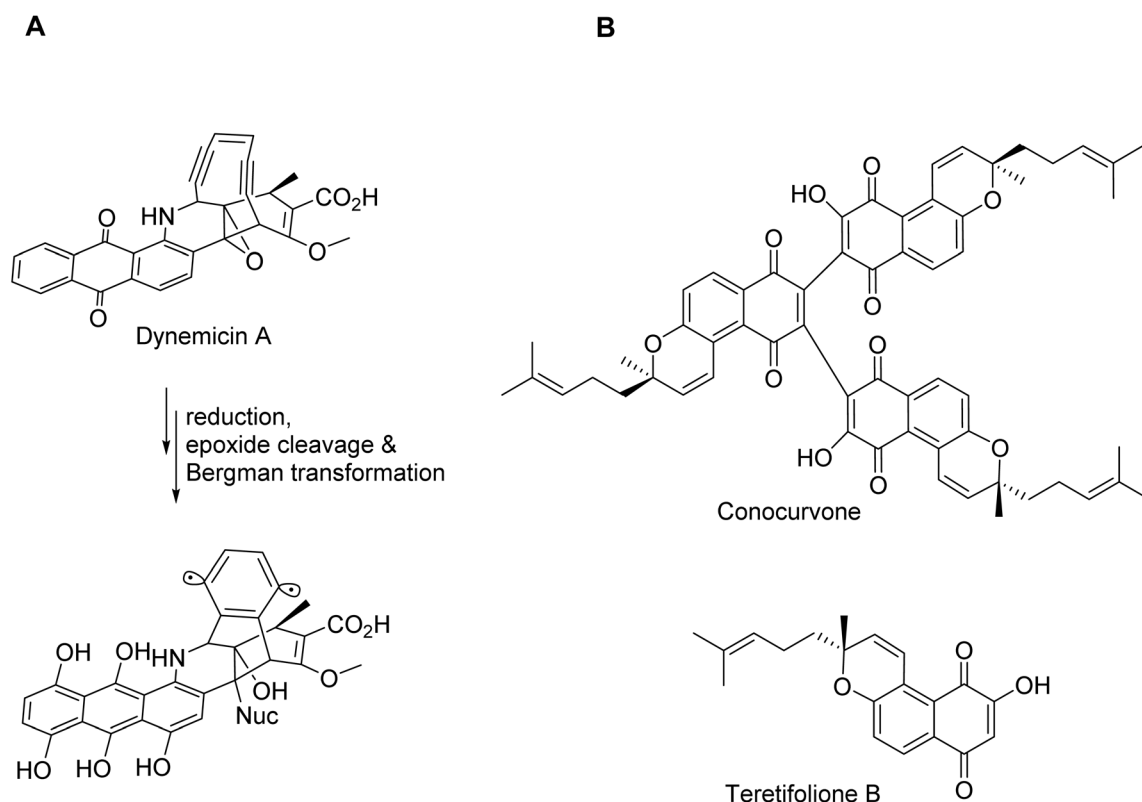
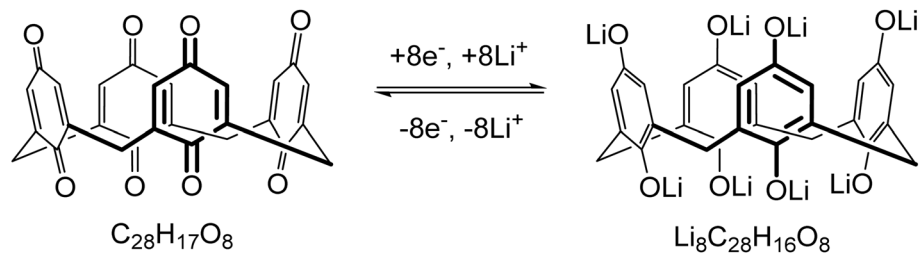


Fig. 4 (A) Dynemicin A, a natural product extracted from microorganism and, (B) Conocurvone, the trimeric form and Teretifolione B, the monomer, isolated from plant extract.





Scheme 4 Quinone-based 3D macromolecular material.

for LIBs. The 3D macromolecular material shown in Scheme 4 has the potential to accept eight electrons with a theoretical capacity of 446 mAh g<sup>-1</sup>.<sup>65</sup> Due to the interesting properties of quinones, it has been made into polymer systems, enabling access to more conventional processes to make electrodes for LIBs. Here these organic based electrodes offer greater versatility compared to mixed metal oxides as they are not cation specific and therefore could be used for both lithium and sodium ion batteries.<sup>66</sup>

As a result of the ease of synthetic chemical transformation of quinone motifs offer, their scalability, biocompatibility, and accessibility from bio-derived or synthetic routes, the potential for quinones to be a viable material for RFB electrolytes is confirmed.

In AORFB systems, 2,7-AQDS (seen in Scheme 2) is considered the state-of-art due to its combination of chemical stability, high solubility, fast redox kinetics and low cost, as reported by Aziz *et al.*<sup>67</sup> This study presents 2,7-AQDS paired with a Br<sub>2</sub>/Br<sup>-</sup> redox couple, achieves a power density of 0.6 W cm<sup>-2</sup> at 1.3 A cm<sup>-2</sup> and over 99% capacity retention per cycle. 2,7-AQDS supports rapid two-electron, two-proton redox reactions in acidic media, with high solubility (>1 M) and ease of structural modification. The system delivers energy densities exceeding 50 Wh L<sup>-1</sup>, rivalling VFBS at a fraction of the cost (\$21 kWh<sup>-1</sup> vs. \$81 kWh<sup>-1</sup>). This breakthrough laid the groundwork for exploring other anthraquinone derivatives with enhanced solubility and redox potentials.

Further innovations in this field have included the synthesis of advanced quinone derivatives, such as 2,6-dihydroxyanthraquinone (2,6-DHAQ) that are isomeric with the alizarin and quinizarin dyes, and offer higher energy densities and improved stability in acidic and neutral conditions.<sup>68,69</sup> Despite the promising advantages of AORFBs, including their environmental friendliness, safety, and tunability, one of the significant challenges is the long-term stability of the organic active materials. Organic molecules used as redox-active species typically can be more susceptible to structural decomposition compared to their inorganic counterparts due to issues such as chemical instability, free radical formation, and side reactions during cycling.<sup>70</sup> This instability not only leads to an increase in capacity fade but also requires higher maintenance costs due to the need for frequent replacement or reconstitution of the active material.

In this review, we aim to explore the degradation mechanisms of quinones in aqueous environment, particularly

focusing on high-performance compounds that exhibit excellent stability over extended cycling of 100–3000 cycles with <0.1% fade rate per day. The degradation pathways of quinones can vary depending on their chemical structure, leading to different reactivity profiles and stability under repeated cycling, which is not well understood. We will evaluate some of these quinones based on their degradation pathways and explore some current strategies to mitigate them. Three major classes of quinones are benzoquinones, naphthoquinones, and anthraquinones (Fig. 2), which are key organic molecules utilized in AORFBs. Variants of this include replacing the benzenoid ring with other heterocycle systems (*i.e.*, thiophene, furan, pyrrole, pyridine *etc.*). The structural variations among these quinones significantly influence their redox and chemical properties, as well as degradation pathways, which are critical for optimizing AORFB performance with a view towards commercial application.

### 3 Degradation mechanisms of quinones

As seen in Scheme 2, quinone molecules undergo redox reactions that involve two electrons and two protons (under acidic conditions), making them efficient charge carriers. They can serve as either anolytes or catholytes depending on their redox potentials and structural modifications, and the choice of the other redox couple in the RFB, though use as an anolyte is most common, especially with an inorganic catholyte.<sup>71,72</sup> In this context, understanding the specific quinone redox couples employed, along with their degradation mechanisms, is crucial for optimizing their performance.

The degradation of quinone-based redox-active species in AORFBs can occur through a number of different pathways, significantly impacting battery performance, as listed in Fig. 5. These degradation pathways lead to capacity loss as the active species concentration is decreased. In the next section, the mechanism and examples of these degradation pathways with reported and typical quinones will be used as illustrative examples to highlight how by-products have been identified, with some potential strategies for mitigation.

#### 3.1 Disproportionation and anthrone formation

Disproportionation and anthrone formation (Scheme 5) occur primarily in anthraquinone-based systems where two semi-



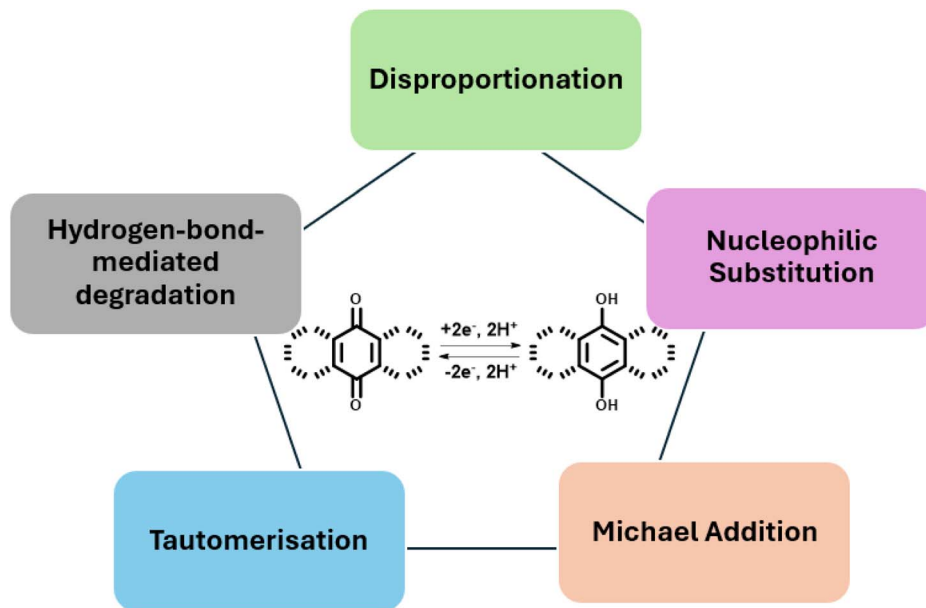


Fig. 5 Generic redox reaction of quinones and degradation pathways of active materials.

hydroquinone molecules can react through two disproportionation pathways involving oxidation and reduction: (1) leading to the formation of the quinone and hydroquinone, and (2) leading to the formation of the quinone (oxidation) and anthrone (reduction) byproduct. In the former the semi-hydroquinone is extremely unstable and reconverts to the quinone and hydroquinone. In the latter pathway, the semi-hydroquinone forms a byproduct anthrone molecule, which cannot be converted back to the quinone and may also undergoes further unwanted reactions reducing the performance of the RFB system.

### 3.1.1 Case studies of disproportionation degradation

**3.1.1.1 2,6-Dihydroxyanthraquinone (2,6-DHAQ).** Goulet *et al.* investigated the degradation mechanisms of 2,6-DHAQ in AORFBs and developed strategies to mitigate capacity fade through redox state management.<sup>73</sup> The study identified irreversible dimerization as the primary degradation pathway, involving the formation of 2,6-dihydroxyanthrone (DHA) *via* reduction of DHAHQ and its subsequent dimerization to (DHA)<sub>2</sub>. This degradation pathway was confirmed using high-resolution mass spectrometry (HRMS), high-performance liquid chromatography-mass spectrometry (HPLC-MS), and <sup>1</sup>H NMR spectroscopy. The authors demonstrated that this mechanism leads to progressive capacity loss, as the conversion of DHAQ to (DHA)<sub>2</sub> replaces the quinone moiety with a benzophenone-like structure, which exhibits higher redox potential, lower energy density, and chemical instability at pH 14.

Insights into this degradation process are shown in Fig. 6C. The accumulation of DHA during symmetric cell cycling was shown by obtaining aliquots and recording changes in the <sup>1</sup>H NMR spectrum over time, with DHA peaks increasing in intensity as cycling progresses. They have quantitatively tracked the conversion of DHAHQ to DHA and subsequently to (DHA)<sub>2</sub>

and correlated the observed capacity fade with the loss of active species.

Quinones such as 2,3- and 2,6-dihydroxyanthraquinone (2,3- and 2,6-DHAQ) are particularly prone to disproportionation reactions (Scheme 6), forming anthrone intermediates that can then undergo dimerization. This process leads to a progressive loss of active quinone content, reducing battery capacity and performance over time.<sup>74</sup> For instance, the disproportionation of 2,6-DHAQ results in the formation of 2,6-dihydroxyanthrone, a precursor to dimerization and electrochemically inactive by-products. This dimerization is particularly detrimental as it not only reduces the number of active redox centres but also contributes to the clogging and fouling of battery components.

The susceptibility of quinone-based systems to redox disproportionation is influenced by the reduction potential of the quinone. Quinones with lower reduction potentials are especially vulnerable to this degradation pathway.<sup>75</sup> In lower-potential quinones, such as 2,6-DHAQ, there is a higher driving force for anthrone formation *via* disproportionation. Chen *et al.* proposed that controlling the pH and modifying the electrolyte environment could significantly reduce the extent of redox disproportionation, thereby enhancing the stability of quinone-based redox couples.<sup>76</sup>

**3.1.1.2 2,3-Dihydroxyanthraquinone (2,3-DHAQ).** Guiheneuf *et al.* introduced 2,3-DHAQ as a promising anolyte for alkaline AORFBs. This compound demonstrated high solubility (0.7 M in 2 M KOH) and suitable redox properties, enabling an Open-Circuit Voltage (OCV) of 1.11 V when paired with potassium ferrocyanide as the catholyte.<sup>22</sup> The flow battery achieved an energy density of 17 Wh L<sup>-1</sup> and maintained a stable Coulombic Efficiency (CE) of over 99.7% during 180 cycles at a current density of 40 mA cm<sup>-2</sup>, with a minimal capacity fade of 0.022% per cycle. Over an extended cycling test of 3000 cycles, the



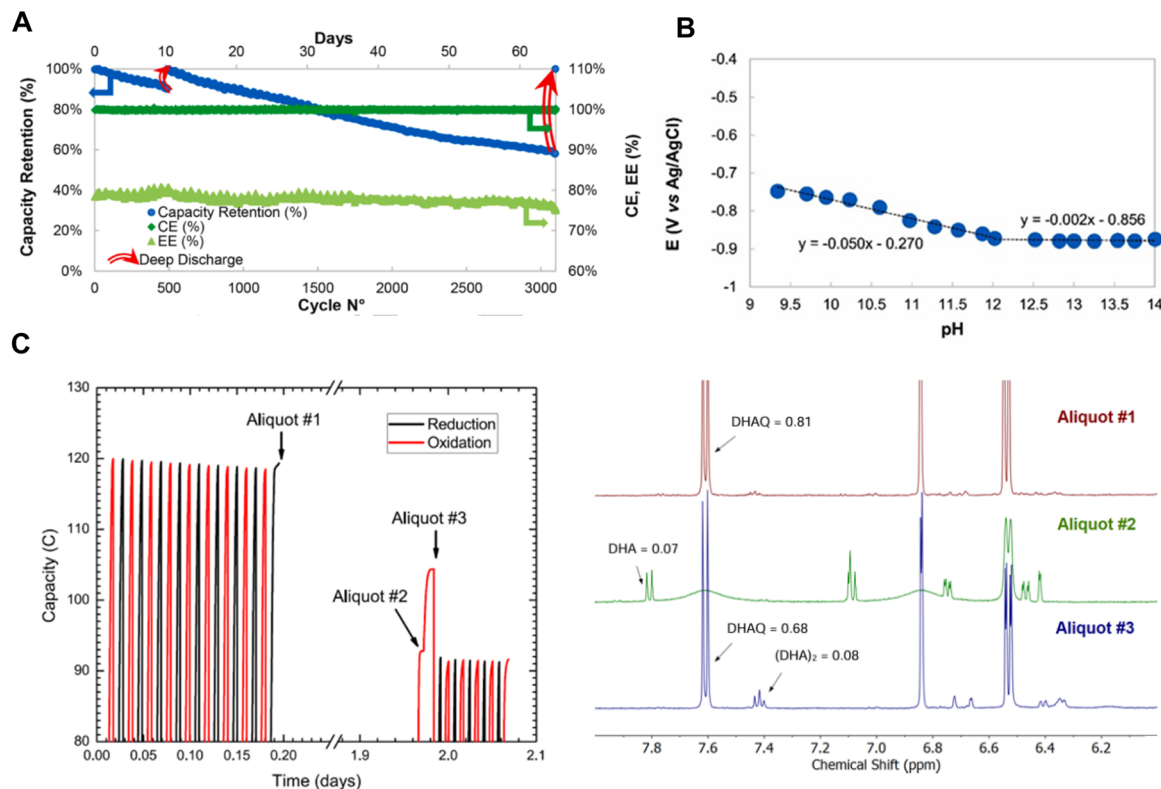
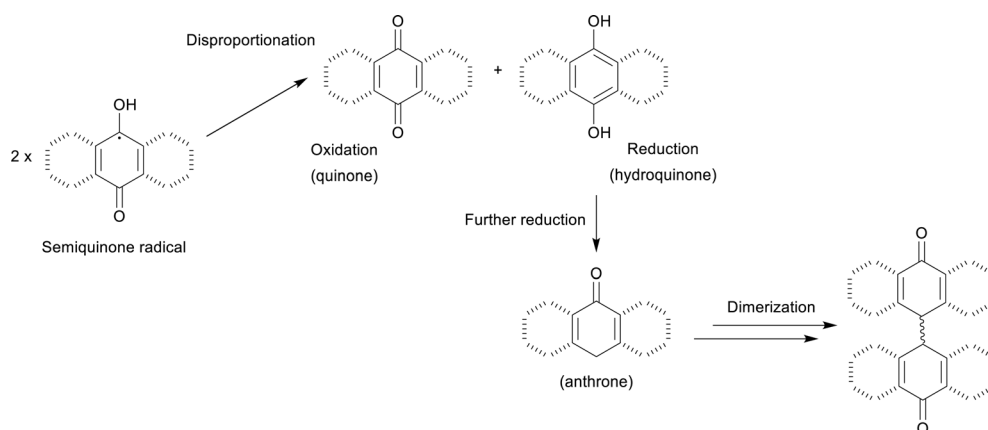


Fig. 6 (A) Long cycle of anolyte solution of 0.2 M 2,3-DHAQ in aqueous KOH 1.8 M (40 mL) and catholyte solution of 0.5 M potassium ferrocyanide in aqueous NaOH 0.2 M (44 mL), displaying Coulombic (CE) and energy efficiencies (EE) and capacity retention against number of cycles. Adapted with permission.<sup>23</sup> Copyright 2022 Elsevier. (B) Pourbaix diagrams of 2,3-DHAQ (containing 1,2-DHAQ) showing the transition of  $2e^-/2H^+$  redox process at  $pH < 12$  to a  $2e^-/0H^+$  process at  $pH > 12$ . (C) Quantitative correlation of DHA formation and subsequent dimerization with capacity loss, when DHAQ electrolyte was held in the reduced state of charge. Adapted with permission.<sup>73</sup> Copyright 2019 The American Chemical Society.

battery displayed reversible capacity fading, retaining full capacity upon deep discharge (Fig. 6A).

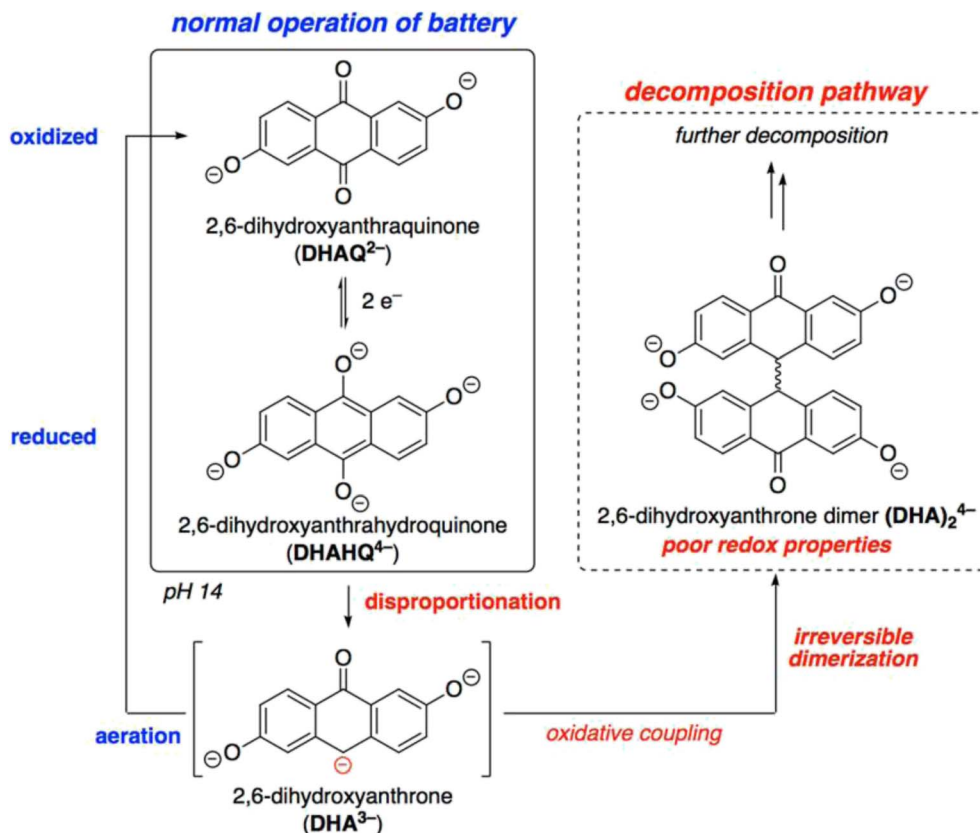
The electrochemical characterization of 2,3-DHAQ revealed a quasi-reversible two-electron redox process at  $-0.85$  V vs. Ag/AgCl. Its diffusion coefficient was measured at  $3.4 \times 10^{-6}$  cm<sup>2</sup> s<sup>-1</sup>, and the electron transfer rate constant was determined to

be  $1.56 \times 10^{-2}$  cm s<sup>-1</sup> confirming fast kinetics. Pourbaix diagrams confirmed its pH-dependent behaviour, with a slope of  $-50$  mV/pH in alkaline conditions indicating a  $2e^-/2H^+$  redox process, transitioning to a  $2e^-/0H^+$  process at higher pH levels (Fig. 6B) as discussed in Scheme 2. The primary degradation pathway of 2,3-DHAQ involves the formation of a non-



Scheme 5 Mechanism showing disproportionation pathway and overreduction of the hydroquinone to form anthrone and further reactions leading to dimer product.





**Scheme 6** Disproportionation degradation pathway leading to irreversible dimerization, applicable to dihydro-quinones such as 2,6-DHAQ. Adapted with permission. Copyright 2019 The American Chemical Society.<sup>73</sup>

electroactive dimer, attributed to a disproportionation-dimerization mechanism (Scheme 5). This process occurs predominantly under high State of Charge (SOC) conditions and elevated cutoff voltages. Mass Spectrometry (MS) and proton nuclear magnetic resonance (<sup>1</sup>H NMR) spectroscopy analysis of post-cycled electrolytes identified the dimeric degradation product which is predicted to form from anthrone intermediates.

**3.1.2 Mitigation of disproportionation degradation.** The finding that dimerization is an irreversible process which occurs readily in lower potential anthraquinones restricts the efforts to further develop such materials. While disproportionation is reversible, two strategies to mitigate this degradation pathway and avoid capacity loss are (i) control of the SOC and (ii) aerating the electrolyte to oxidize DHA back to DHAQ. By restricting the SOC to 88% instead of cycling to full

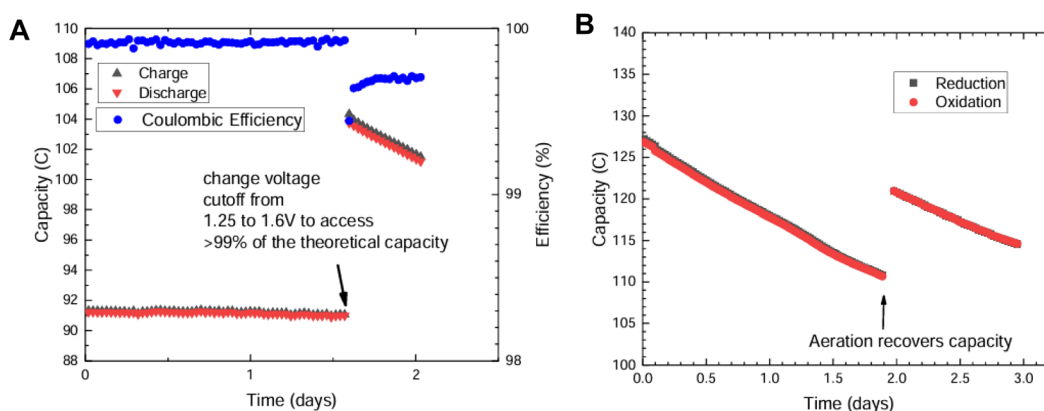


**Fig. 7** (A) Limiting the state of charge (SOC) reduces the rate of capacity loss in an anolyte-limited DHAQ-Fe(CN)<sub>6</sub> full cell. (B) Recovery of 70% of lost capacity in which the capacity-limiting side (5 mL of 0.1 M DHAQ in a 1.2 M KOH solution) is aeration after discharging in a symmetric cell cycle. Adapted with permission.<sup>73</sup> Copyright 2019 The American Chemical Society.



capacity, the fade rate was reduced from 5.6% per day to 0.14% per day, as shown in Fig. 7A. This strategy does not completely eliminate its formation unless a SOC below 60% is utilized. To prevent dimerization of DHA into (DHA)<sub>2</sub> upon anthrone formation, aeration of the discharged electrolyte enabled recovery of up to 70% of lost capacity by converting DHA to DHAQ under aerobic conditions (Fig. 7B). This study emphasizes the trade-off between redox potential and molecular stability, as lowering the reduction potential of anthraquinones increases their propensity for disproportionation. These findings underscore the importance of managing redox states and designing operating conditions to balance stability and performance in organic RFBs. Goulet *et al.*<sup>73</sup> projected that the combination of SOC control and aeration could reduce capacity fade rates by two orders of magnitude, making quinone-based RFBs viable for long-term grid-scale energy storage.

### 3.2 Nucleophilic substitution

Nucleophilic substitution involves nucleophiles such as water or hydroxide ion attacking the electrophilic carbons, leading to hydroxylated intermediates, giving byproducts with very different properties to the starting quinone.

Nucleophilic substitution thus affects the stability and performance of quinone-based AORFBs. Nucleophilic substitution primarily occurs in alkaline conditions where hydroxide ions can attack heteroatom-linked solubilizing groups or carbonyl groups in the quinone structure (Scheme 7). Quinones with substituents such as sulfonates and ethers exhibit enhanced water solubility but are more prone to nucleophilic attack. This results in the cleavage of these functional groups, leading to decreased solubility and irreversible capacity fading. For instance, Kwabi *et al.* summarized that nucleophilic attack of AQDS is time-dependent, with prolonged exposure to reactive hydroxide ions reducing the quinone's redox activity and long-term performance.<sup>38</sup>

Hydrolytic degradation, a form of nucleophilic substitution, is another critical pathway, particularly under pH-neutral conditions. Water molecules can react with the carbonyl groups of quinone compounds, leading to hydrolysis and the formation of electrochemically inactive by-products. This mechanism is especially prevalent in derivatives such as 2,2'-((9,10-dioxo-9,10-dihydroanthracene-1,4-diyl)bis(azanediyl))bis(*N,N,N*-trimethylethan-1-aminium)dichloride (BDEAQCl<sub>2</sub>) (Fig. 8), where hydrolytic side reactions contribute significantly to capacity loss during battery cycling. Xu *et al.* noted

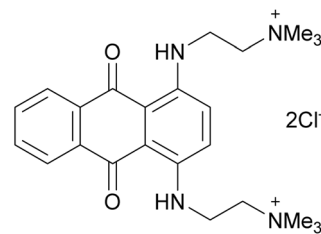


Fig. 8 1,4-BDEAQCl<sub>2</sub> chemical structure.

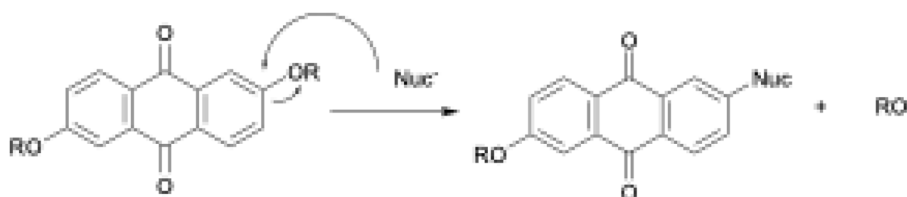
substantial hydrolytic degradation of BDEAQCl<sub>2</sub> in neutral pH systems, highlighting the importance of mitigating such reactions to preserve battery efficiency.<sup>77</sup>

To counteract nucleophilic substitution, molecular engineering approaches have focused on stabilizing the ether linkages and reducing nucleophilic susceptibility. Alfaraidi *et al.*<sup>78</sup> demonstrated that introducing -NH<sub>2</sub> groups adjacent to ether-linked substituents in anthraquinone derivatives significantly suppressed nucleophilic attacks. This NH<sub>2</sub>-substituted anthraquinone exhibited high solubility (1.1 M) and excellent cycling performance, achieving a CE exceeding 99.8% and minimal capacity fading over extended cycles. These results highlight the effectiveness of functional group optimization in enhancing molecular stability under alkaline conditions.

Similarly, hydrolytic degradation can be mitigated through non-hydrolyzable functional groups. By modifying quinone derivatives with hydrophilic chains, researchers have developed electrolytes with improved resistance to water-induced degradation. Such modifications prevent the formation of inactive by-products and prolong the functional lifetime of quinone-based systems, making them more viable for long-term energy storage applications.<sup>79</sup>

#### 3.2.1 Case studies of nucleophilic substitution

**3.2.1.1 4,4'-((9,10-Anthraquinone-2,6-diyl)dioxy)dibutyrate (2,6-DBEAQ).** The study conducted by Kwabi *et al.* demonstrates the use of 4,4'-((9,10-anthraquinone-2,6-diyl)dioxy)dibutyrate (2,6-DBEAQ) in RFBs at pH 12, achieving remarkable stability and solubility.<sup>80</sup> The innovative functionalization of 2,6-DHAQ with carboxylate terminal groups improved its solubility to 0.6 M at pH 12 and 1.1 M at pH 14, significantly outperforming its precursor, 2,6-DHAQ. When paired with potassium ferri/ferrocyanide as the catholyte this system achieved an open-circuit voltage of over 1 V and a theoretical energy density of 17 Wh L<sup>-1</sup> at pH 12. Symmetric cell cycling tests revealed an extraordinary capacity fade rate of less than 0.01% per day or <0.001% per cycle. Electrochemical studies of 2,6-DBEAQ



Scheme 7 Mechanism for nucleophilic substitution of hydroxide releasing an alkoxide group. Mechanism similar for other functional groups.



showed a high diffusion coefficient of  $1.58 \times 10^{-6} \text{ cm}^2 \text{ s}^{-1}$  and good chemical stability and redox reversibility. The separation between its two redox potentials,  $E_1$  and  $E_2$  (see Scheme 2), was reduced to 6 mV compared to 60 mV in 2,6-DHAQ, minimizing the life-time of the reactive semiquinone radicals and enhancing the overall active materials' stability. Polarization studies of full cells demonstrated near-linear voltage-current relationships, achieving a peak galvanic power density of  $0.24 \text{ W cm}^{-2}$  at 100% SOC. Over five days of cycling (250 cycles) at 100

$\text{mA cm}^{-2}$ , the battery retained 99.94% current efficiency and experienced a minimal capacity fade of 0.05% per day (Fig. 9A).

Despite its exceptional performance, 2,6-DBEAQ exhibits degradation primarily through the cleavage of its  $\gamma$ -hydroxybutyrate functional groups in the oxidized state, catalyzed by hydroxide ions in highly alkaline environments (Scheme 8). Elevated temperature stability tests demonstrated a half-life of approximately five years at pH 14 and 0.1 M concentration at room temperature. This degradation mechanism is concentration and pH-dependent, with slower degradation at pH 12

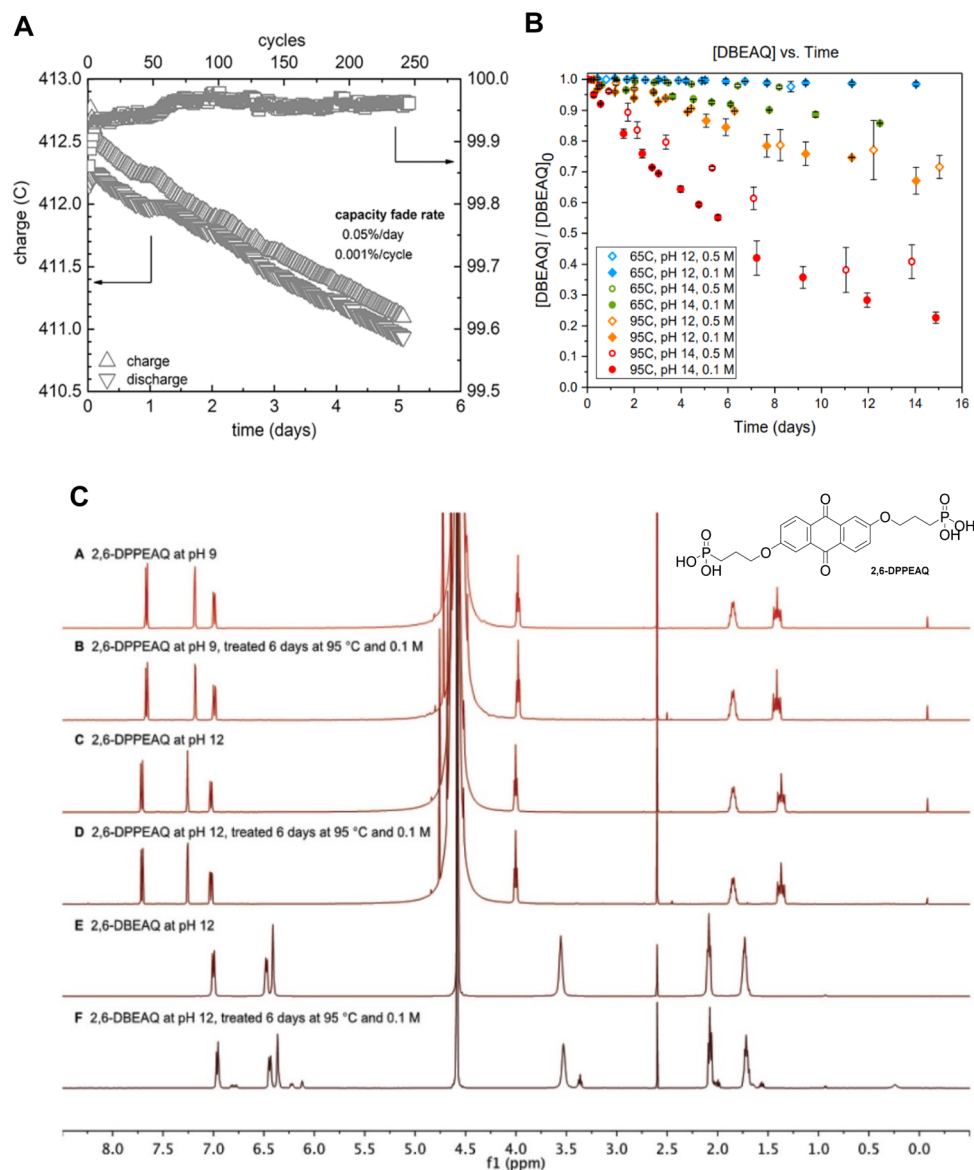
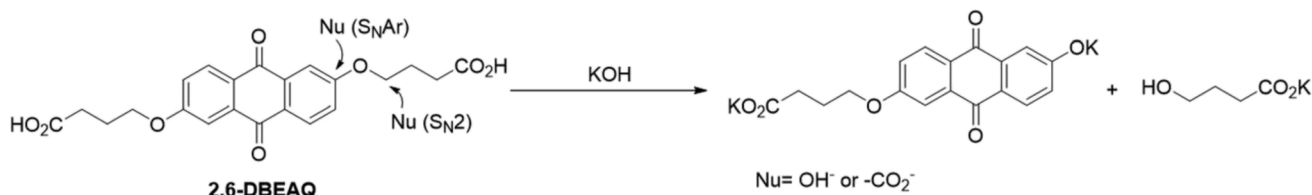


**Fig. 9** (A) Current efficiency (squares) and charge (upward-pointing triangles) and discharge (downward pointing triangles) capacity versus time and cycle number for a cell comprising of anolyte, 5 mL of 0.5 M 2,6-DBEAQ at pH 12 and catholyte of 30 mL of 0.3 M potassium ferrocyanide and 0.1 M potassium ferricyanide at pH 12. The cell was cycled galvanostatically at  $100 \text{ mA cm}^{-2}$  between 1.4 and 0.6 V, and each half cycle ended with a potentiostatic hold until the magnitude of the current density fell below  $2 \text{ mA cm}^{-2}$ . (B) Time course of 2,6-DBEAQ decomposition at various temperature (65 °C and 95 °C), pH (pH 12 and pH 14), and concentration conditions (0.1 M and 0.5 M). Adapted with permission.<sup>80</sup> Copyright 2018 Cell Press. (C) <sup>1</sup>H NMR spectra (500 MHz, 10 mM NaCH<sub>3</sub>SO<sub>3</sub> internal standard, δ 2.6 ppm) comparing of the stability of 2,6-DPPEAQ with respect to alkyl chain cleavage at pH 9 and 12 to that of 2,6-DBEAQ at pH 12, all at 0.1 M quinone concentration in aqueous solution. Adapted with permission.<sup>81</sup> Copyright 2019 Wiley.





Scheme 8 Possible degradation nucleophilic substitution mechanism of ether-linked quinones. Example above is for 2,6-DBEAQ.

compared to pH 14 (Fig. 9B). The oxidative decomposition pathways were confirmed through  $^1\text{H}$  NMR spectroscopy and time-course studies. In contrast to its precursor, 2,6-DHAQ, the reduced form of 2,6-DBEAQ, demonstrated superior stability due to the increased thermodynamic stability of the hydroquinone core and reduced susceptibility to semi-hydroquinone radical formation. Computational studies corroborated these findings, indicating that alkyl chain functionalization improved the molecule's thermodynamic resistance to degradation by hydroxide or hydrolytic cleavage.

Low-permeability membranes, such as the Fumasep E-600 series, played a critical role in minimizing crossover of 2,6-DBEAQ and ferricyanide species. These membranes exhibited extremely low permeabilities of  $5.26 \times 10^{-13} \text{ cm}^2 \text{ s}^{-1}$  for 2,6-DBEAQ, ensuring minimal reactant crossover and minimal capacity fade due to leakage. This research highlights the potential of 2,6-DBEAQ for long-lifetime, high-performance aqueous organic RFBs and underscores the need for further molecular optimization to mitigate oxidative degradation and extend operational lifetimes.

**3.2.1.2 ((9,10-Dioxo-9,10-dihydroanthracene-2,6-diyl)bis(oxy))bis(propane-3,1-diyl))bis(phosphonic acid) (2,6-DPPEAQ).** Ji *et al.* introduced a phosphonate-functionalized anthraquinone, 2,6-DPPEAQ (see Fig. 9), as a highly stable redox-active anolyte for AORFBs operating at near-neutral pH.<sup>81</sup> The functionalization with phosphonic acid groups also significantly improved the solubility and stability of 2,6-DPPEAQ at pH 9, enabling operation in less alkaline conditions compared to its predecessor, 2,6-DBEAQ (see Scheme 8). The solubility of 2,6-DPPEAQ was measured to be 0.75 M at pH 9, translating to a theoretical volumetric capacity of  $40.2 \text{ Ah L}^{-1}$ . This phosphonate-functionalized quinone achieved a record-low-capacity fade rate of 0.00036% per cycle (0.014% per day), corresponding to a projected annual fade rate of only 5.0% under typical operating conditions.

The degradation of 2,6-DPPEAQ was studied extensively at different pH levels and temperatures. The stability of 2,6-DPPEAQ and 2,6-DBEAQ under thermal stress at pH 14 (95 °C for 5.5 days) revealed that both molecules experienced 45% decomposition. The  $^1\text{H}$  NMR for 2,6-DPPEAQ revealed cleavage products consistent with phosphonate side-chain degradation. In contrast, 2,6-DBEAQ displayed cleavage of carboxylate groups, which occurred more readily under these conditions. At a lower pH (pH 9) and elevated temperature of 65 °C, 2,6-DPPEAQ exhibited no measurable degradation over six days, demonstrating superior stability compared to its predecessor (Fig. 9C).

While 2,6-DPPEAQ in the oxidized form displayed minor degradation, the reduced form remained chemically stable at pH 14 and 65 °C over two weeks. No significant decomposition products for the reduced form were detected in the  $^1\text{H}$  NMR, underscoring the robustness of the phosphonate-functionalized molecule under alkaline conditions. This stability difference highlights the importance of redox state management in minimizing degradation during cycling.

Electrochemical performance tests confirmed the durability of 2,6-DPPEAQ in a full-cell configuration with a ferro/ferricyanide catholyte. Galvanostatic cycling showed negligible capacity fade over 480 cycles, with no detectable decomposition in the anolyte by NMR, cyclic voltammetry (CV), or UV-Vis spectroscopy. Additionally, no crossover products in the membrane-separated flow cell were detected, further supporting the exceptional retention of electroactive species.

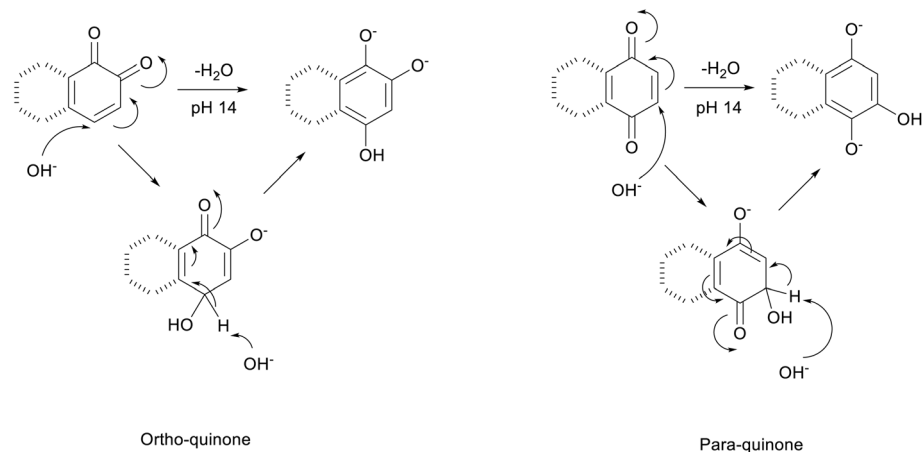
### 3.2.2 Mitigation of nucleophilic substitution degradation.

The position of functional groups on quinone molecules significantly affects their stability and solubility. Hasan *et al.* showed that the introduction of hydrophilic substituents in the  $\beta$ -position of quinones enhanced solubility and stability, improving battery performance.<sup>82</sup> Similarly, Gerken *et al.* demonstrated that substituting all possible C-H positions on the quinone molecule with sulfonated thioether groups resulted in tetrasubstituted quinones, such as TSPSQ, that showed greater resistance to degradation.<sup>83</sup> These modifications effectively protected reactive sites, thereby preventing nucleophilic substitution and improving the long-term stability of quinone-based electrolytes.

The type of functional groups attached to quinone molecules also significantly impact their stability, redox potential, and solubility. Functionalization with hydrophilic groups, such as sulfonate or phosphonate groups, has been used to enhance the solubility of quinones in aqueous electrolytes while reducing their susceptibility to nucleophilic attack. For instance, Jing *et al.* introduced non-hydrolyzable side chains to anthraquinones which improved the solubility and stability of these molecules in aqueous solutions.<sup>84</sup> These functional groups effectively shield reactive sites and reduce the propensity for hydrolytic and nucleophilic degradation, leading to improved long-term cycling stability.

The study using 2,6-DPPEAQ addressed degradation related to oxygen ingress. The authors observed pH oscillations between 9 and 12 during cycling, which were reversible when oxygen was excluded but became irreversible due to hydroquinone oxidation *via* oxygen reduction reactions (ORR) when oxygen was present. This illustrates the effect of oxygen on





**Scheme 9** Mechanism showing the addition of hydroxide ion to *ortho*- and *para*-quinones where the product will now have different chemical, physical and electrochemical properties to the initial quinone compound.

stability, emphasizing the need for inert gas purging to prevent irreversible degradation.

### 3.3 Michael addition

Michael addition occurs when nucleophiles such as amines or thiols attack the  $\beta$ -carbon, forming adducts that alter the symmetry of the molecule, redox potential and functionality (*i.e.* solubility).

Michael addition represents a critical degradation mechanism in quinone-based AORFBs, that is exacerbated by disproportionation reactions. Quinones, as a Michael acceptor, are highly susceptible to nucleophilic attack, particularly from water or hydroxide ions (Scheme 9). Michael addition reactions significantly impact the longevity of quinone-based electrolytes by reducing active species concentration, altering electron delocalization, and promoting the formation of insoluble by-products. This reaction leads to the formation of an inactive adduct that irreversibly reduces the concentration of active redox species, thereby decreasing electrochemical efficiency and causing capacity fade during long-term cycling.

Benzoquinones, due to a number of highly reactive electrophilic sites, are especially vulnerable to Michael addition. Gerken *et al.* reported that quinones paired with high-potential catholytes experience significant degradation through this pathway, resulting in oligomerization and the generation of high-molecular-weight by-products under acidic conditions.<sup>41</sup> These by-products not only deplete active quinone species but also accumulate within the battery, potentially fouling the system's components and further impairing performance.

#### 3.3.1 Case studies of Michael addition degradation

**3.3.1.1 Phoenicin.** A study conducted by Wilhelmsen *et al.*<sup>85</sup> presented a detailed investigation into phoenicin, a bis-synthesized bis-quinone derived from *Penicillium phoeniceum*, and evaluated its performance as an anolyte for alkaline AORFBs. The battery configuration consisted of  $1.48 \times 10^{-2}$  M phoenicin as the anolyte with a ferrocyanide catholyte in 1 M KOH. The OCV was recorded at 0.86 V, and the initial charge capacity was measured at  $1.58 \text{ Ah L}^{-1}$ , which aligns well with

the theoretical capacity of  $1.64 \text{ Ah L}^{-1}$ , indicating a four-electron transfer per bis-quinone unit. Galvanostatic cycling of the battery confirmed that it sustained 1111 charge-discharge cycles over 13 days, achieving an average coulombic efficiency of 99.27%. However, as seen in Fig. 10A, progressive capacity loss was observed, with a total of 78% capacity fade over the testing period, equating to a 6.2% daily degradation rate or 0.071% per cycle. The voltage plateaus showed an initial charge potential of 0.86 V, which later stabilized at 0.77 V, suggesting changes in redox-active species over multiple cycles.

A major challenge identified in this study was the instability of phoenicin in alkaline conditions, with degradation occurring primarily *via* Michael addition. Michael addition alters the molecular structure of phoenicin (Scheme 10), leading to the formation of hydroxylated derivatives, hydroquinone forms, and polymerized oligomers, which reduce the availability of electrochemically active species over time. The degradation mechanism was examined by  $^1\text{H}$  NMR spectroscopy, which revealed a gradual disappearance of quinone ring proton signals as the reaction progressed. This indicated the conversion of phoenicin into hydroxylated and oligomerized forms, which exhibit significant different redox properties. Additionally, LC-MS analysis confirmed that Michael addition leads to the accumulation of hydroxylated derivatives, such as oosporein ( $\text{C}_{14}\text{H}_{10}\text{O}_8$ ), along with larger oligomeric structures including dimers, trimers, tetramers, and pentamers.

The electrochemical effects of degradation were examined using CV and rotating disk electrode (RDE) studies. The CV experiments showed that after 14 hours in 1 M KOH, an additional reduction peak appeared, corresponding to newly formed redox-inactive species (Fig. 10B). Further evidence of degradation was provided by RDE studies, which showed that the diffusion coefficient of phoenicin decreased from  $7.71 \times 10^{-6} \text{ cm}^2 \text{ s}^{-1}$  to  $4.93 \times 10^{-6} \text{ cm}^2 \text{ s}^{-1}$ , indicating the formation of oligomeric degradation products exhibiting slower mass transfer. The Tafel plot and Butler-Volmer analysis confirmed an increase in charge transfer resistance, further contributing to capacity fade. This study is particularly important as it not



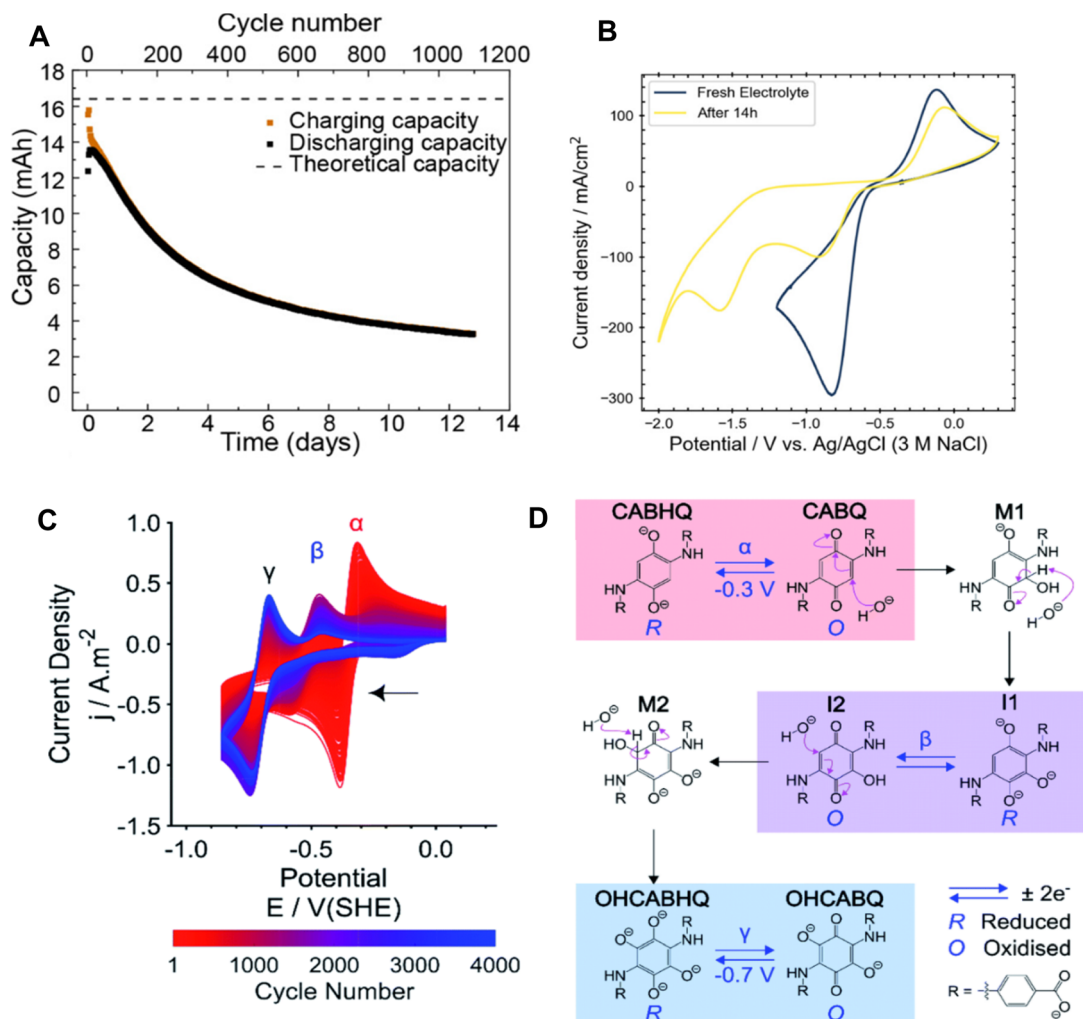
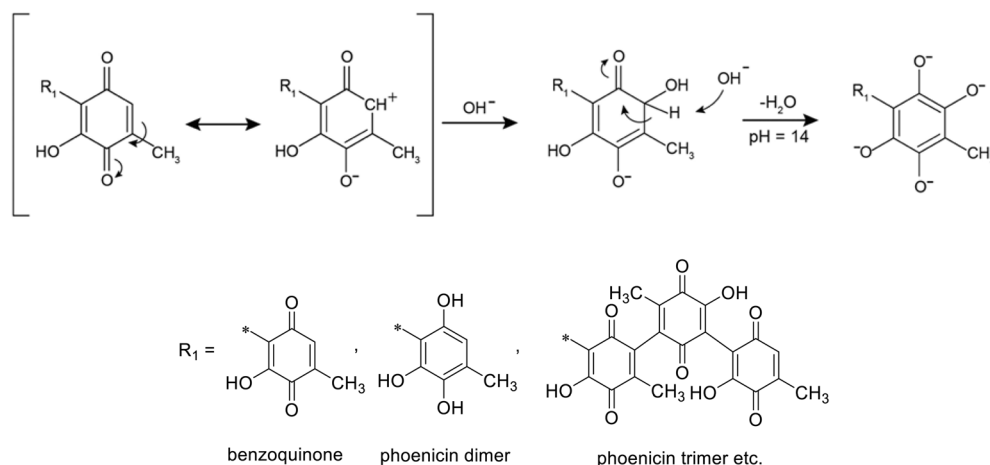


**Fig. 10** (A) Full cell performance with 10 mL of  $1.48 \times 10^{-2}$  M phenicin as anolyte and 22 mL of 0.17 M ferrocyanide/0.03 M ferricyanide as catholyte. (B) Cyclic voltammograms of fresh (blue line) and after being stored for 14 h (yellow line) electrolyte of  $4.78 \times 10^{-3}$  M phenicin in 1 M KOH. Adapted with permission.<sup>85</sup> Copyright 2023 The American Chemical Society. (C) Cyclic voltammograms of 1 mM CABQ in 1 M KOH/D<sub>2</sub>O. (D) Proposed reaction mechanism of CABQ that undergoes stepwise hydroxylation at the 3 and 6 positions, forming the redox-active stable product, OHCABQ. The corresponding electrochemical conversions in the CV,  $\alpha$ ,  $\beta$ , and  $\gamma$  are labelled in the mechanism. Adapted with permission.<sup>86</sup> Copyright 2021 Royal Society of Chemistry.



**Scheme 10** Possible degradation products of phenicin via Michael addition.



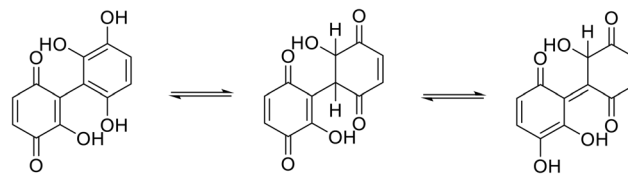
only highlights the high initial electrochemical efficiency of phenocin but also addresses its degradation challenges, particularly Michael addition-induced structural transformations that lead to capacity fade.

**3.3.1.2 2,5-(4-Carboxyanilino)-1,4-benzoquinone (CABQ).** A study by Jethwa *et al.* (2021)<sup>86</sup> investigated 2,5-(4-carboxyanilino)-1,4-benzoquinone (CABQ), an amine-functionalized benzoquinone, as an anolyte for AORFBs. CABQ undergoes a unique hydrogen bond-mediated conjugate addition, which results in a stable hydroxylated product rather than irreversible degradation. The electrochemical performance of CABQ was evaluated in an alkaline redox flow battery setup using 1 M KOH as the supporting electrolyte (Fig. 10C and D). The battery used  $1.48 \times 10^{-2}$  M CABQ as the anolyte and 0.17 M ferrocyanide/0.03 M ferricyanide as the catholyte. The OCV was measured at 1.1 V, and the initial charge capacity was determined to be  $3.5 \text{ Ah L}^{-1}$ , corresponding to a two-electron transfer per quinone unit.

Galvanostatic cycling of the battery achieved 600 stable cycles, with an average coulombic efficiency of 99.72%. The charge–discharge curves revealed three distinct voltage plateaus at 1.00 V, 1.15 V, and 1.38 V, corresponding to the stepwise oxidation–reduction processes of CABQ (Fig. 10C). The first plateau corresponds to the formation of the radical anion (CABSQ<sup>3-</sup>), the second is the formation of the hydroquinone form (CABHQ<sup>4-</sup>), and the third to the stabilization of OHCABQ (3,6-dihydroxy-2,5-(4-carboxyanilino)-1,4-benzoquinone), the electrochemically and redox-active form. The proposed degradation pathway (Fig. 10D) involves initially the two-electron reduction of CABQ to form the hydroquinone state (CABHQ), followed by hydroxylation selectively at the 3 and 6 positions, leading to the formation of an intermediate conjugate addition products (M1, I1 and I2) and upon deprotonation and tautomerization, forms OHCABQ (Fig. 10D). However, despite the stability of CABQ, prolonged cycling resulted in gradual capacity fade, which was attributed to the formation of OHCABQ, rather than irreversible molecular decomposition. Using CV, *in situ* and *ex situ* NMR, EPR spectroscopy, and density functional theory (DFT) modelling, the study provides a comprehensive understanding of CABQ's performance in AORFB.

**3.3.2 Mitigation of Michael addition degradation.** In addition to hydrophilic functional groups which can prevent nucleophilic attack, modifying quinones with sterically hindering substituents can also provide enhanced stability against Michael addition. The introduction of bulky substituents limits the accessibility of nucleophiles to reactive sites on the quinone molecule, thus reducing the rate of degradation. This approach has proven successful in stabilizing anthraquinone derivatives, resulting in improved CEs and reduced capacity fading over multiple cycle.<sup>87</sup>

Researchers have also introduced sulfonated thioether substituents to mitigate this pathway of degradation. By blocking reactive electrophilic sites on quinone molecules, these substituents reduce the tendency for nucleophilic attack and oligomer formation.<sup>88</sup> Tetrasubstituted benzoquinones, similar structure to TSPSQ, incorporating four sulfonated



Scheme 11 Possible tautomeric species occurring via presence of multiple quinone moieties.

thioether groups, exhibited significantly enhanced chemical stability, enabling long-term operation in acidic media.<sup>41</sup>

### 3.4 Tautomerization and hydrogen bonding

Tautomerization plays a critical role in the degradation of quinone-based anolytes, affecting their electrochemical stability, charge retention, and long-term viability in AORFBs. Typically, protons catalyze the tautomerization between keto and enol forms, leading to structural rearrangement (sometimes driven by sterics) and changes in electronic distribution. Although tautomerization is often reversible in organic molecules, electrochemical cycling conditions can drive irreversible transformations, forming redox-inactive by-products and precipitates, ultimately resulting in permanent material loss (Scheme 11). The ability of quinone anolytes to undergo repeated redox cycling without experiencing molecular rearrangement is essential for maintaining high-performance flow batteries, making the study of tautomerization crucial for designing durable and efficient electrolytes.

The susceptibility of quinone-based anolytes to tautomerization is highly dependent on structural modifications, pH conditions, and molecular interactions within the electrolyte. Quinones with hydroxyl (–OH) and carboxyl (–COOH) functional groups are particularly vulnerable, as these groups facilitate intramolecular hydrogen bonding, stabilizing the enol form while destabilizing the active quinone state. Research has shown that this tautomeric shift leads to the accumulation of redox-inactive diketone species, reducing the effective concentration of electroactive material and accelerating capacity fade over extended cycling.<sup>38,89</sup> Additionally, tautomerization-induced transformations often increase molecular hydrophobicity, leading to reduced solubility and precipitation, further contributing to electrolyte instability. This effect is especially pronounced in naphthoquinone-based anolytes, where electron-donating groups enhance the likelihood of tautomeric rearrangement.

A striking example of tautomerization-induced degradation occurs in Bislawsonone, where hydroquinone tautomerizes to form di- and tetra-ketone structures, rendering the species electrochemically inactive. This process leads to progressive capacity loss, as the transformed molecules can no longer participate in redox reactions. Spectroscopic techniques such as NMR and HPLC have provided direct evidence of tautomerization-induced molecular degradation, confirming that intramolecular rearrangement is a dominant factor in anolyte instability. Additionally, computational studies indicate



that quinones with high redox potentials are more prone to tautomerization, especially when hydroxyl groups are in conjugation with carbonyl moieties, promoting electronic delocalization and accelerating structural rearrangement.<sup>90,91</sup>

### 3.4.1 Case studies of tautomerization degradation

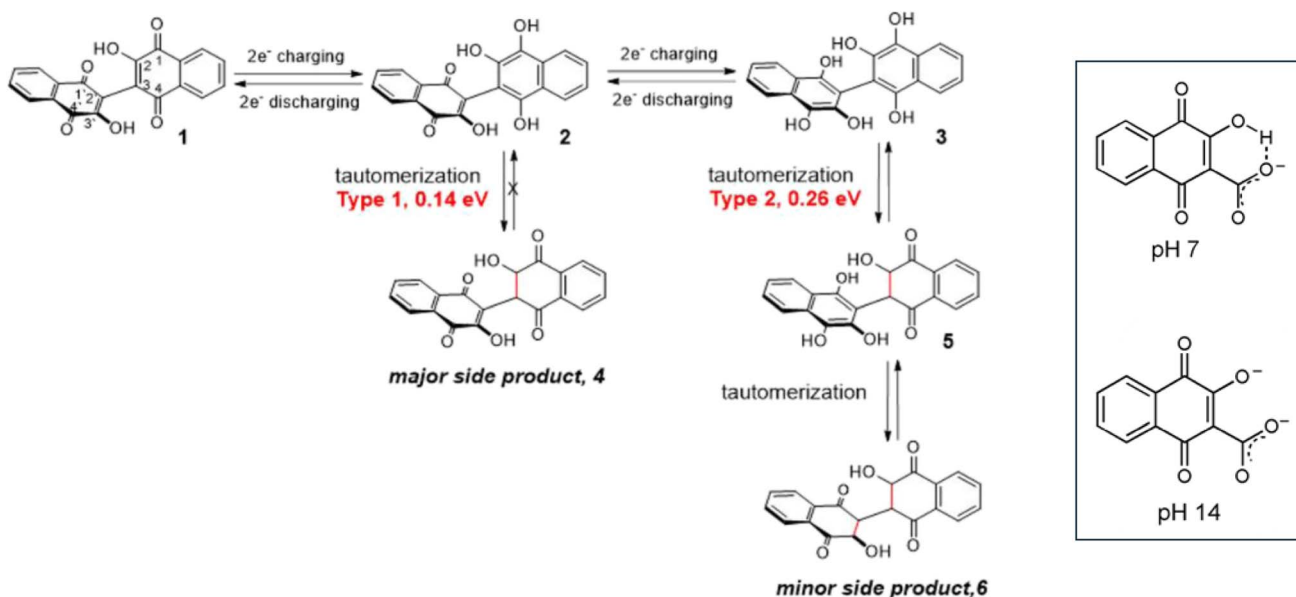
#### 3.4.1.1 2,2'-Bis(3-hydroxy-1,4-naphthoquinone) (Bislawson)

Tong *et al.* introduced Bislawson, a naphthoquinone dimer, as a high-performance redox-active anolyte for alkaline AORFBs.<sup>92</sup> This dimerization strategy improved solubility, stability, and permeability compared to the Lawsonsone monomer. Bislawson demonstrated a high solubility of 0.56 M in 1 M KOH, corresponding to 2.24 M electrons or 60 Ah L<sup>-1</sup>. In a flow cell paired with potassium ferrocyanide as the catholyte, it achieved an OCV of 1.05 V, a peak power density of 0.28 W cm<sup>-2</sup>, and a round-trip energy efficiency of 79.3%. At a concentration of 0.5 M, the cell achieved 98.3% of theoretical capacity and cycled stably at 300 mA cm<sup>-2</sup>, retaining 95.5% of capacity utilization. Coulombic efficiency remained consistently above 99.5% during 6.8 days of cycling, with a capacity fade rate of 0.74% per day or 0.038% per cycle.

Electrochemical characterization of Bislawson showed reversible 4-electron redox activity at a reduction potential of -0.551 V vs. SHE, which was 50 mV more negative than the monomer. Rotating disk electrode measurements revealed a diffusion coefficient of 4.54 × 10<sup>-6</sup> cm<sup>2</sup> s<sup>-1</sup>, while viscosity remained below 2 cP up to the solubility limit in 1 M KOH, minimizing energy losses due to pumping. The permeability of Bislawson through Fumasep E-620K membranes was an order of magnitude lower than that of Lawsonsone, confirming the advantage of the dimerization approach.

The primary degradation mechanism of Bislawson involves enol-ketone tautomerization of its reduced form to produce a diketone structure, 2,3-dihydrobislawson (Scheme 12) which was confirmed by <sup>1</sup>H NMR. This tautomerization process reduces redox activity and leads to capacity loss over time. Peaks corresponding to aliphatic protons in the diketone were observed, indicating the loss of conjugation and the redox-inactive nature of the degradation product. To further validate the product of this mechanism, LC-High Resolution MS was used to identify the diketone form (*m/z* = 347.0559) as the dominant degradation product.

Time-course NMR analysis tracked the progressive conversion of Bislawson into its diketone form, showing a gradual increase in the relative intensity of degradation product signals over 21 days. Quantitative NMR revealed that the diketone accounted for 14.2% of the total NMR-active material after this period. The precipitation of redox-inactive degradation products was identified as the cause of capacity loss, highlighting the impact of reduced solubility in alkaline environments. Finally, molecular dynamics simulation of the tautomerization process was conducted, confirming the susceptibility of the reduced form of Bislawson to enol-ketone transformation and precipitation under cycling conditions. Additional insights into the degradation process by demonstrating the effect of pH on the rate of tautomerization was also provided. The study showed that the reduced form (compound 3, Scheme 12) of Bislawson exhibits increased degradation rates in higher pH environments due to the enhanced nucleophilicity of hydroxide ions, which catalyse the enol-ketone tautomerization. Thus, this highlights the importance of pH optimization as a strategy to mitigate degradation and extend operational lifetimes.



**Scheme 12** . A schematic representation of the decomposition pathway *via* keto-enol tautomerisation of the reduced forms of Bislawson. The red text are the calculated reaction energies for the tautomerization, derived using the B3LYP/6-311+G(d,p) (PCM) level of theory. These energy values are the variation between the ground-state energies of the tautomerization side products and the reduced form, suggesting quantitative insights of the thermodynamic favourability of the degradation mechanism. Adapted with permission.<sup>92</sup> Copyright 2019 The American Chemical Society. (inset) Proposed ionized structure after the reduction of 2,3-HCNQ at pH 14.



Theoretical calculations predicted that Bislawsonone is less thermodynamically susceptible to tautomerization than lawsone due to its protective dimeric structure. However, the study identified eight Bislawsonone derivatives with enhanced stability and comparable reduction potentials. These derivatives, featuring oxy-alkyl substitutions at the various positions of the aromatic rings, hold promise for further improving the stability of naphthoquinone-based AORFBs.

**3.4.1.2 2-Hydroxy-3-carboxy-1,4-naphthoquinone (2,3-HCNQ).** Wang *et al.* developed a high-performance AORFB using 2-hydroxy-3-carboxy-1,4-naphthoquinone (2,3-HCNQ) as the redox-active anolyte and potassium ferrocyanide as the catholyte (inset, Scheme 12).<sup>93</sup> Functionalizing 2-hydroxy-1,4-naphthoquinone (2-HNQ, Lawsone) with a carboxylic acid group significantly enhanced the solubility, stability, and electrochemical performance of the molecule. The solubility of 2,3-HCNQ was measured at 1.2 M in 1.0 M KOH, corresponding to a theoretical volumetric capacity of 53.6 Ah L<sup>-1</sup>, a considerable improvement over the 0.48 M solubility of 2-HNQ. The AORFB achieved an OCV of 1.02 V and delivered a peak power density of 0.255 W cm<sup>-2</sup>. Galvanostatic cycling tests at 100 mA cm<sup>-2</sup> demonstrated excellent stability, with a CE of close to 100% and an energy efficiency of 68.8% over 100 cycles. The initial discharge capacity of 18.8 Ah L<sup>-1</sup> was retained at 94.7% after 100 cycles, resulting in a fade rate of 3.4% per day.

The primary degradation mechanism of 2,3-HCNQ involves chemical decomposition of its reduced form at high SOC conditions. Symmetric flow cell tests indicated that the reduced form of 2,3-HCNQ exhibited a fade rate of 13.4% per day at 100% SOC, compared to 0.6% per day at 0% SOC. In the proposed degradation pathways, they highlighted the role of intramolecular hydrogen bonding and electrochemical deprotonation in stabilizing the molecule under alkaline conditions. They have suggested that the reduced form of 2,3-HCNQ may not be fully deprotonated in the alkaline solution, due to the formation of intramolecular hydrogen bonds and the restraint of already dissociated dianion structure of the charged carboxylate and phenolate groups which repel each other (inset, Scheme 12). The reduced form undergoes side reactions in highly alkaline environments, leading to capacity loss and diminished electrochemical reversibility. These results underscore the critical role of SOC management in extending the lifespan of AORFBs utilizing 2,3-HCNQ.

The introduction of the carboxylic acid group in 2,3-HCNQ not only improved solubility but also reduced the likelihood of disproportionation reactions. Comparative studies with 2-HNQ highlighted the superior stability of 2,3-HCNQ, as 2-HNQ suffered significant capacity loss due to oxygen-induced side reactions and its limited solubility. Electrochemical studies revealed a two-electron redox process for 2,3-HCNQ, with a formal potential of  $-0.73$  V *versus* Ag/AgCl in 1.0 M KOH. The molecule displayed rapid redox kinetics, characterized by a diffusion coefficient of  $3.44 \times 10^{-6}$  cm<sup>2</sup> s<sup>-1</sup> and a rate constant ( $k_0$ ) of  $2.07 \times 10^{-3}$  cm s<sup>-1</sup>, outperforming many common inorganic redox-active cations and demonstrating its viability as an anolyte material.

**3.4.2 Mitigation of tautomerization degradation.** To mitigate tautomerization-induced degradation, molecular engineering strategies have been explored to enhance structural stability and extend the lifespan of quinone-based anolytes. Introducing electron-withdrawing functional groups such as sulfonic acids ( $-\text{SO}_3\text{H}$ ) and phosphonic acids ( $-\text{PO}_3\text{H}_2$ ) next to the phenolic group has proven effective in stabilizing quinones by reducing electron density around the carboxylic groups, thereby suppressing tautomeric shifts. Additionally, steric hindrance modifications, such as alkoxy substitutions, prevent intramolecular hydrogen bonding, a key driver of tautomerization-induced degradation. For example, 2,6-diphosphonate-functionalized anthraquinone (2,6-DPPEAQ) has demonstrated exceptional resistance to tautomerization, maintaining long-term cycling stability even under near-neutral pH conditions. Another promising approach is optimizing electrolyte composition through buffered systems and pH control, which has been shown to minimize tautomerization-induced rearrangements.

## 4 Conclusion

Tapping the full potential of quinones will rely upon a series of advances that address some of the problems discussed in this review with existing and emerging tools. Quinone-based AORFBs have immense potential for large-scale energy storage, thanks to the affordability, tunability, and sustainability of the active material. However, their long-term stability remains a challenge and addressing the degradation mechanisms discussed in this review will play a major part.

High-performing quinones in AORFBs exhibit key characteristics that enhance electrochemical stability, energy density, and long-term cycling durability. High solubility ( $>0.5$  M) is crucial for maximizing volumetric capacity, with functional groups such as hydroxyl ( $-\text{OH}$ ), carboxyl ( $-\text{COOH}$ ), phosphonate ( $-\text{PO}_3\text{H}_2$ ), and sulfonate ( $-\text{SO}_3\text{H}$ ) improving water miscibility and electrolyte utilization, as seen in 2,3-HCNQ and 2,6-DBEAQ. The use of water solubilizing functional groups needs to be balanced with the effect that such groups have on degradation mechanisms, both due to stability of functional groups, and the effect on redox potential to increase maximum theoretical cell voltage in aqueous solution. Supramolecular interactions such as  $\pi$ - $\pi$  stacking, which may lead to precipitation at higher concentrations also need to be factored in, as does the pH of the aqueous solution. There are recent examples of stable redox reversibility ensures prolonged cycling, with optimized redox potentials ( $-0.5$  V to  $+0.8$  V *vs.* SHE) balancing charge efficiency and degradation resistance, as demonstrated by 2,6-DPPEAQ ( $-0.49$  V *vs.* SHE) and 2,3-HCNQ ( $-0.73$  V *vs.* SHE). The multiple factors that need to be balanced should lead to a greater role of theoretical calculations and machine learning led approaches to assist in molecular design in the coming years, and the challenge will proposing new structures that are still synthetically accessible at an affordable price while meeting these criteria.

Degradation mechanisms like disproportionation, nucleophilic substitution, Michael addition, tautomerization and





**Table 2** Comparison of redox-active organic molecules for AORFBs, summarizing key properties such as concentration, fade rates, degradation mechanisms, performance highlights, and strategies proposed for improvement. This table highlights the advancements in solubility, stability, and electrochemical behaviour achieved through molecular design and operational optimizations

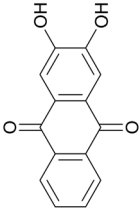
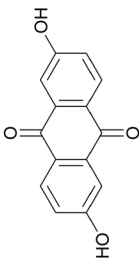
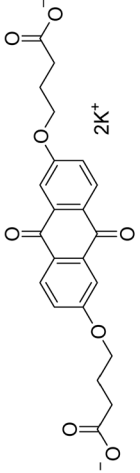
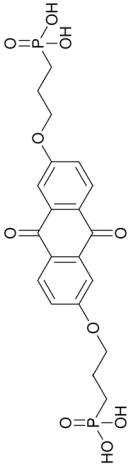
Active material	Concentration	Fade rate	Degradation mechanisms	Key findings	Improvements/strategies	Ref.
<p><b>2,3-Dihydroxyanthraquinone (2,3-DHAQ)</b></p> 	0.7 M in KOH (37.5 Ah L <sup>-1</sup> )	~0.016% per cycle over 3000 cycles	Disproportionation and dimerization at high SOC forming (DHA) <sub>2</sub>	Stable cycling over 3000 cycles; minimal capacity fade; reversible degradation mechanisms	Deep discharge to recover capacity; limiting SOC; membrane optimization to reduce crossover	22
<p><b>2,6-Dihydroxyanthraquinone (2,6-DHAQ)</b></p> 	0.5 M in 1 M KOH	5.6% per day (high SOC), 0.14% per day (88% SOC)	Disproportionation to form DHA; irreversible dimerization into (DHA) <sub>2</sub>	SOC control reduced fade from 5.6% to 0.14% per day; aeration recovered 70% lost capacity	SOC restriction to prevent high-potential degradation; aeration to reverse disproportionation effects	73
<p><b>4,4'-((9,10-Anthraquinone-2,6-diyloxy)dibutyrate (2,6-DBEAQ)</b></p> 	1.1 M at pH 14, 0.6 M at pH 12	<0.01% per day, <0.001% per cycle	Hydrolytic cleavage of $\gamma$ -hydroxybutyrate groups <i>via</i> hydroxide attack	Record-low fade rates; stable cycling at pH 12–14; high solubility improves energy density	pH optimization to balance solubility/stability; molecular modifications to suppress hydrolytic cleavage	80
<p><b>2,6-Diphosphonate-functionalized anthraquinone (2,6-DPPEAQ)</b></p> 	0.75 M at pH 9 (40.2 Ah L <sup>-1</sup> )	0.00036% per cycle (~5% per year)	Cleavage of phosphonate side chains under highly alkaline conditions	Exceptional stability in near-neutral pH; negligible fade; 480 stable cycles; energy efficiency ~70%	Redox state management; near-neutral pH operation minimizes degradation; optimized cell design to prevent oxygen ingress	81

Table 2 (Contd.)

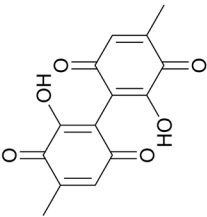
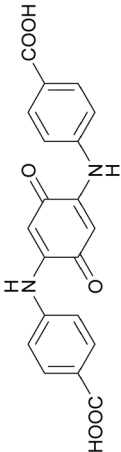
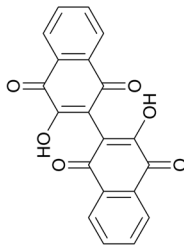
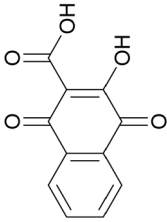
Active material	Concentration	Fade rate	Degradation mechanisms	Key findings	Improvements/strategies	Ref.
<p><b>Phoenicin</b></p> 	0.2 M in 2.1 M KOH	2.85% per day (0.35% per cycle)	Michael addition at $\beta$ -position; oxidized form more prone to degradation	Biologically derived; stable in reduced form; coulombic efficiency $\sim 98.5\%$ ; moderate performance with $11.75 \text{ Ah L}^{-1}$ initial capacity	Operate in reduced state; minimize oxidized exposure; potential for biosynthetic optimization	85
<p><b>2,5-(4-Carboxyanilino)-1,4-benzoquinone (CABQ)</b></p> 	0.066 M in 1 M KOH ( $3.5 \text{ Ah L}^{-1}$ )	High-capacity fade observed, 0.0226 mAh per cycle with dual NAFION layers	Conjugate (Michael) addition followed by dihydroxylation; formation of OH-CABQ	Undergoes spontaneous nucleophilic attack forming stable lower-potential product; high coulombic efficiency ( $\sim 99.7\%$ ) with 3 plateaus observed	Dual membrane to limit crossover; substitution at 3,6-positions to block addition; operate post-conversion to OH-CABQ	86
<p><b>2,2'-Bis(3-hydroxy-1,4-naphthoquinone) (Bislawson)</b></p> 	0.56 M in 1 M KOH ( $60 \text{ Ah L}^{-1}$ )	0.008% per cycle (low conc.), 0.038% per cycle (high conc.)	Enol-ketone tautomerization forms redox-inactive diketones; precipitation of byproducts	Improved solubility/stability; nonplanar structure minimizes permeability; 97.7% theoretical capacity utilized	Rational molecular design targeting tautomerization resistance; computational derivatives for enhanced stability	92
<p><b>2-Hydroxy-3-carboxy-1,4-naphthoquinone (2,3-HCNQ)</b></p> 	1.2 M in 1 M KOH ( $53.6 \text{ Ah L}^{-1}$ )	3.4% per day	Decomposition of reduced form under high SOC conditions; oxygen-induced side reactions	High solubility; peak power density $0.255 \text{ W cm}^{-2}$ ; 94.7% capacity retention after 100 cycles	SOC management; optimization of functional groups to suppress side reactions; improved membrane selectivity	93



Table 3 Glossary of names, structures and abbreviations

Abbreviation	Name	Structure
AQ	Anthracene-9,10-dione(anthraquinone)	
2,7-AQDS	9,10-Dioxo-9,10-dihydroanthracene-2,7-disulfonic acid	
1,4-BDEAQCl <sub>2</sub>	2,2'-((9,10-dioxo-9,10-dihydroanthracene-1,4-diyl)bis(azanediyl))bis( <i>N,N,N</i> -trimethylethan-1-aminium)dichloride	
Bislawson	2,2'-Bis(3-hydroxy-1,4-naphthoquinone)	
CABQ	2,5-(4-Carboxyanilino)-1,4-benzoquinone	
2,3-DAD	Benzo[ <i>g</i> ]phthalazine-5,10-dione	
2,6-DBEAQ	4,4'-(2,6-((Diyl)dioxy)dibutyrate))-9,10-anthraquinone	
2,6-DHA	2,6-Dihydroxyanthracen-9(10 <i>H</i> )-one	
(DHA) <sub>2</sub>	2,2',6,6'-Tetrahydroxy-[9,9'-bianthracene]-10,10'(9 <i>H</i> ,9' <i>H</i> )-dione (2,6-dihydroxyanthrone dimer)	

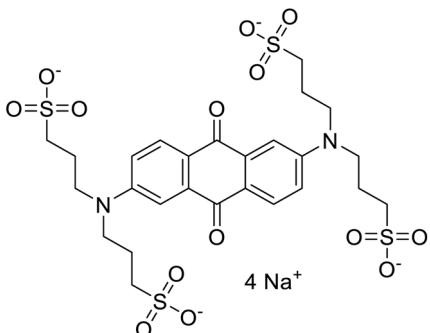
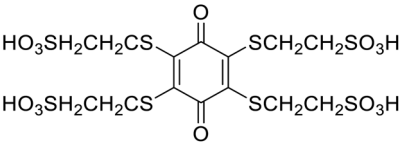
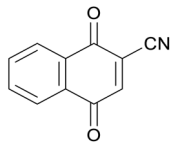
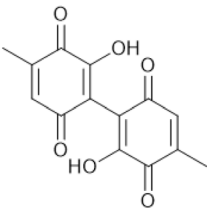


Table 3 (Contd.)

Abbreviation	Name	Structure
DHAHQ	Anthracene-2,6,9,10-tetraol (2,6-dihydroxyanthrahydroxyquinone)	
2,3-DHAQ	2,3-Dihydroxyanthraquinone	
2,6-DHAQ	2,6-Dihydroxyanthraquinone	
2,6-DPPEAQ	(((9,10-Dioxo-9,10-dihydroanthracene-2,6-diyl)bis(oxy))bis(propane-3,1-diyl))bis(phosphonic acid)	
2,3-HCNQ	2-Hydroxy-3-carboxy-1,4-naphthoquinone	
2-HNQ (Lawsone)	2-Hydroxy-1,4-naphthoquinone	
HQS	Potassium 2,5-dihydroxybenzenesulfonate	
OHCABQ	4,4'-((2,5-Dihydroxy-3,6-dioxocyclohexa-1,4-diene-1,4-diyl)bis(azanediyl))dibenzoic acid	
OHCABHQ	4,4'-((2,3,5,6-Tetrahydroxy-1,4-phenylene)bis(azanediyl))dibenzoic acid	



Table 3 (Contd.)

Abbreviation Name	Structure
TSAQ  ((9,10-Anthraquinone-2,6diyl)bis(azanetriyl)) tetrakis(propane-1-sulfonate)	
TSPSQ  2,2',2'',2'''-(3,6-Dioxocyclohexa-1,4-diene-1,2,4,5-tetrayl)tetrakis(sulfanediyl)) tetrakis(ethane-1-sulfonic acid)	
QCN  1,4-Dioxo-1,4-dihydronaphthalene-2-carbonitrile	
n/a  Phoenicin	

hydrogen-bond-mediated degradation gradually reduce battery efficiency, causing capacity loss and limiting their commercial viability. Resistance to degradation can be achieved through steric hindrance, blocking functional groups, and hydrophobic modifications, effectively mitigating hydrolysis and oxidative degradation, with 2,6-DBEAQ and 2,6-DPPEAQ setting benchmarks for record-low fade rates. Operating stability in near-neutral to alkaline pH (7–14) enhances electrolyte compatibility and minimizes decomposition, as seen in 2,6-DPPEAQ and 2,6-DBEAQ, which resist oxygen-induced side reactions. Moreover, commercial viability is strengthened by cost-effective synthesis, scalable molecular modifications (e.g., PEGylation and phosphonation for solubility), and simple precursor availability, making quinones ideal candidates for next-generation flow battery applications.

Understanding these degradation pathways is crucial for improving active material lifetime and ensuring sustainable battery operation. Various analytical techniques have been employed to monitor, characterize, and mitigate degradation processes, offering insights into molecular stability, decomposition pathways, and electrolyte longevity. These techniques

include NMR, EPR, UV-Vis and electrochemical methods, and some in-depth reviews of these techniques have recently been published.<sup>6,94–97</sup> In RFBS, the further development of *in operando* techniques is essential not only to monitor but more importantly identification of the intermediates and degradation products that can also feed into molecular design strategies.

Researchers have made impressive progress by varying quinone structures, tweaking electrolyte compositions, and applying real-time monitoring techniques to track molecular changes, albeit in a non-systematic approach. Investigation like functional group modifications, pH studies, and redox state management have led to more stable quinone derivatives with enhanced cycling lifetimes. Notably, compounds like 2,6-DHAQ, 2,6-DBEAQ, and 2,6-DPPEAQ have demonstrated remarkable durability, with some formulations showing minimal capacity fade over thousands of cycles. A summary of the quinones discussed in this review is shown in Table 2, with an explanation of degradation mechanisms, key findings, and strategies used to improve performance, which may act as a blueprint for other studies in the future. In addition, having



standard assays and benchmark materials would facilitate better comparisons of novel anolyte and catholyte systems, with standard measurement parameters allowing for better comparisons to be made between materials and RFB configurations.

Recent advancements in the design of heterocyclic quinones<sup>35</sup> have demonstrated the large material possibilities yet to be fully explored, but offer possible solutions by addressing challenges related to solubility, redox stability, and degradation resistance of current polyaromatic cyclic structures. A study on nitrogen-rich fused heteroaromatic quinones introduced structural modifications have produced materials with enhanced electron delocalization, reduce nucleophilic attack, and improve solubility in aqueous media.<sup>35</sup> Also, a solubility prediction model was developed to facilitate the discovery of highly soluble and stable quinone derivatives by integrating substitution pattern and functional group identity.<sup>98</sup> This approach significantly outperformed conventional quantum chemical solubility estimations, enabling the prediction of 808 new anthraquinone derivatives with high accuracy, and this method of targeted research may become more common to move beyond more simple functionalization of quinone aromatic rings.

With ongoing research, quinone-based AORFBs could soon match or even outperform traditional metal-based systems like vanadium redox flow batteries. The key to unlocking their full potential lies in further refining molecular design, electrolyte engineering, and integrating *in situ* diagnostics, and using nature inspired strategies will also have a place.<sup>99</sup> If these challenges are addressed, quinone-based AORFBs could revolutionize energy storage by providing safe, cost-effective, and scalable solutions for a renewable-powered future. The road ahead is promising science in bringing us closer to truly sustainable, long-duration energy storage, and quinones might just be the breakthrough we need. For a glossary of names, structures and abbreviations see Table 3.

## Author contributions

Afzal: writing – original draft. Heshan Liyanaarachchi: writing – original draft. Gavin E. Collis: conceptualization, supervision, writing – review and editing. Lathe A. Jones: conceptualization, supervision, writing – review and editing. Subashani Maniam: conceptualization, supervision, writing – review and editing.

## Conflicts of interest

There are no conflicts to declare.

## Data availability

No primary research results, software or code have been included and no new data were generated or analysed as part of this review.

## Notes and references

- 1 A. Shahsavari and M. Akbari, *Renewable Sustainable Energy Rev.*, 2018, **90**, 275–291.
- 2 D. A. Elalfy, E. Gouda, M. F. Kotb, V. Bureš and B. E. Sedhom, *Energy Strategy Rev.*, 2024, **54**, 101482.
- 3 Z. Yang, J. Zhang, M. C. W. Kintner-Meyer, X. Lu, D. Choi, J. P. Lemmon and J. Liu, *Chem. Rev.*, 2011, **111**, 3577–3613.
- 4 P. Leung, A. A. Shah, L. Sanz, C. Flox, J. Morante, Q. Xu, M. Mohamed, C. P. De León and F. Walsh, *J. Power Sources*, 2017, **360**, 243–283.
- 5 L. Zhang, R. Feng, W. Wang and G. Yu, *Nat. Rev. Chem.*, 2022, **6**, 524–543.
- 6 P. Arévalo-Cid, P. Dias, A. Mendes and J. Azevedo, *Sustainable Energy Fuels*, 2021, **5**, 5366–5419.
- 7 Z. Deller, L. A. Jones and S. Maniam, *Green Chem.*, 2021, **23**, 4955–4979.
- 8 Y. Liu, Q. Chen, P. Sun, Y. Li, Z. Yang and T. Xu, *Mater. Today Energy*, 2021, **20**, 100634.
- 9 M. Pan, M. Shao and Z. Jin, *SmartMat*, 2023, **4**, e1198.
- 10 Z. Zhao, X. Liu, M. Zhang, L. Zhang, C. Zhang, X. Li and G. Yu, *Chem. Soc. Rev.*, 2023, **52**, 6031–6074.
- 11 F. Zhu, Q. Chen and Y. Fu, *Green Energy Environ.*, 2024, **9**, 1641–1649.
- 12 M. Yang, L. Chen, J. Wang, G. Msigwa, A. I. Osman, S. Fawzy, D. W. Rooney and P.-S. Yap, *Environ. Chem. Lett.*, 2023, **21**, 55–80.
- 13 A. Cannon, S. Edwards, M. Jacobs, J. W. Moir, M. A. Roy and J. A. Tickner, *RSC Sustainability*, 2023, **1**, 2092–2106.
- 14 J. Doyle, Galvanic Battery, *US Pat.*, US224404, 1880.
- 15 M. Skyllas-Kazacos, *J. Electrochem. Soc.*, 2022, **169**, 070513.
- 16 Y. Tolmachev, *Flow Batteries From 1879 To 2022 And Beyond*, Qeios, 2022, p. 1, DOI: [10.32388/G6G4EA](https://doi.org/10.32388/G6G4EA).
- 17 A. Aluko and A. Knight, *IEEE Access*, 2023, **11**, 13773–13793.
- 18 S. Maniam, *Batteries: the Future of Energy Storage*, CRC Press, 2024.
- 19 F. Zhang, M. Gao, S. Huang, H. Zhang, X. Wang, L. Liu, M. Han and Q. Wang, *Adv. Mater.*, 2022, **34**, 2104562.
- 20 J. D. Hofmann, F. L. Pfanschilling, N. Krawczyk, P. Geigle, L. Hong, S. Schmalisch, H. A. Wegner, D. Mollenhauer, J. Janek and D. Schröder, *Chem. Mater.*, 2018, **30**, 762–774.
- 21 M. R. Gerhardt, L. Tong, R. Gómez-Bombarelli, Q. Chen, M. P. Marshak, C. J. Galvin, A. Aspuru-Guzik, R. G. Gordon and M. J. Aziz, *Adv. Energy Mater.*, 2017, **7**, 1601488.
- 22 S. Guiheneuf, T. Godet-Bar, J. M. Fontmorin, C. Jourdin, D. Floner and F. Geneste, *J. Power Sources*, 2022, **539**, 231600.
- 23 S. Guiheneuf, A. Lê, T. Godet-Bar, L. Chancelier, J. M. Fontmorin, D. Floner and F. Geneste, *ChemElectroChem*, 2021, **8**, 2526–2533.
- 24 P. A. White, G. E. Collis, M. Skidmore, M. Breedon, W. D. Ganther and K. Venkatesan, *New J. Chem.*, 2020, **44**, 7647–7658.
- 25 Y. Ding, C. Zhang, L. Zhang, Y. Zhou and G. Yu, *Chem. Soc. Rev.*, 2018, **47**, 69–103.
- 26 C. Wiberg, T. J. Carney, F. Brushett, E. Ahlberg and E. Wang, *Electrochim. Acta*, 2019, **317**, 478–485.



- 27 R. C. Prince, P. L. Dutton and M. R. Gunner, *Biochim. Biophys. Acta, Bioenerg.*, 2022, **1863**, 148558.
- 28 D. R. Weinberg, C. J. Gagliardi, J. F. Hull, C. F. Murphy, C. A. Kent, B. C. Westlake, A. Paul, D. H. Ess, D. G. McCafferty and T. J. Meyer, *Chem. Rev.*, 2012, **112**, 4016–4093.
- 29 P. S. Guin, S. Das and P. C. Mandal, *Int. J. Electrochem.*, 2011, **2011**, 816202.
- 30 T. D. Chung, *Bull. Korean Chem. Soc.*, 2014, **35**, 3143–3155.
- 31 J. D. Hofmann and D. Schröder, *Chem. Ing. Tech.*, 2019, **91**, 786–794.
- 32 H. Wang, S. Y. Sayed, E. J. Lubber, B. C. Olsen, S. M. Shirurkar, S. Venkatakrishnan, U. M. Tefashe, A. K. Farquhar, E. S. Smotkin, R. L. McCreery and J. M. Buriak, *ACS Nano*, 2020, **14**, 2575–2584.
- 33 V. Singh and H. R. Byon, *ACS Appl. Energy Mater.*, 2024, **7**, 7562–7575.
- 34 G. Longatte, O. Buriez, E. Labbé, M. Guille-Collignon and F. Lemaître, *ChemElectroChem*, 2024, **11**, e202300542.
- 35 R. B. Jethwa, D. Hey, R. N. Kerber, A. D. Bond, D. S. Wright and C. P. Grey, *ACS Appl. Energy Mater.*, 2024, **7**, 414–426.
- 36 M. Chen, R. Chen, I. Zhitomirsky, G. He and K. Shi, *Mater. Sci. Eng., R*, 2024, **161**, 100865.
- 37 D. Emmel, S. Kunz, N. Blume, Y. Kwon, T. Turek, C. Minke and D. Schröder, *Nat. Commun.*, 2023, **14**, 6672.
- 38 D. G. Kwabi, Y. Ji and M. J. Aziz, *Chem. Rev.*, 2020, **120**, 6467–6489.
- 39 G. Yang, Y. Zhu, Z. Hao, Q. Zhang, Y. Lu, Z. Yan and J. Chen, *Adv. Energy Mater.*, 2024, **14**, 2400022.
- 40 C. Xie, Y. Duan, W. Xu, H. Zhang and X. Li, *Angew. Chem., Int. Ed.*, 2017, **56**, 14953–14957.
- 41 J. B. Gerken, C. W. Anson, Y. Preger, P. G. Symons, J. D. Genders, Y. Qiu, W. Li, T. W. Root and S. S. Stahl, *Adv. Energy Mater.*, 2020, **10**, 2000340.
- 42 S. Bauer, J. C. Namyslo, D. E. Kaufmann and T. Turek, *J. Electrochem. Soc.*, 2020, **167**, 110522.
- 43 K. Lourenssen, J. Williams, F. Ahmadpour, R. Clemmer and S. Tasnim, *J. Energy Storage*, 2019, **25**, 100844.
- 44 S. H. Qazi, R. C. Rodríguez and L. Vandavelde, *Proceedings of the International Conference on Sustainability: Developments and Innovations*, 2024, pp. 53–60.
- 45 C. Xie, H. Zhang, W. Xu, W. Wang and X. Li, *Angew. Chem.*, 2018, **130**, 11341–11346.
- 46 W. Lee, G. Park and Y. Kwon, *Chem. Eng. J.*, 2020, **386**, 123985.
- 47 M. Wu, M. Bahari, Y. Jing, K. Amini, E. M. Fell, T. Y. George, R. G. Gordon and M. J. Aziz, *Batteries Supercaps*, 2022, **5**, e202200009.
- 48 L. F. Fieser and M. Fieser, *Organic Chemistry*, Chapman and Hall, New York, 3rd edn, 1956.
- 49 I. D. Rattee, *Chem. Soc. Rev.*, 1972, **1**, 145–162.
- 50 P. S. Vankar, R. Shanker, D. Mahanta and S. C. Tiwari, *Dyes Pigm.*, 2008, **76**, 207–212.
- 51 T. F. G. G. Cova, A. A. C. C. Pais and J. S. Seixas de Melo, *Sci. Rep.*, 2017, **7**, 6806.
- 52 K.-Y. Choi, *Dyes Pigm.*, 2020, **181**, 108570.
- 53 X. Gong, R. Gutala and A. K. Jaiswal, in *Vitamins & Hormones*, Academic Press, 2008, vol. 78, pp. 85–101.
- 54 L. Styer, *Biochemistry*, New York, San Francisco, 3rd edn, 1988.
- 55 T. Eisner and J. Dean, *Proc. Natl. Acad. Sci. U. S. A.*, 1976, **73**, 1365–1367.
- 56 D. J. Aneshansley, T. Eisner, J. M. Widom and B. Widom, *Science*, 1969, **165**, 61–63.
- 57 E. Price and S. Johnson, *Quinones: Occurrence, Medicinal Uses and Physiological Importance*, Nova Publishers, 2013.
- 58 L. Zhang, G. Zhang, S. Xu and Y. Song, *Eur. J. Med. Chem.*, 2021, **223**, 113632.
- 59 H. Laatsch, *Angew. Chem. Int. Ed. Engl.*, 1994, **33**, 422–424.
- 60 B. Halton, A. J. Kay and Z. Zhi-mei, *J. Chem. Soc., Perkin Trans. 1*, 1993, 2239–2240.
- 61 W. Ng and D. Wege, *Tetrahedron Lett.*, 1996, **37**, 6797–6798.
- 62 G. E. Collis, D. Jayatilaka and D. Wege, *Aust. J. Chem.*, 1997, **50**, 505–514.
- 63 A. S. Devlin and J. Du Bois, *Chem. Sci.*, 2013, **4**, 1059–1063.
- 64 K. N. Winzenberg, P. Kemppinen, G. Fanchini, M. Bown, G. E. Collis, C. M. Forsyth, K. Hegedus, T. B. Singh and S. E. Watkins, *Chem. Mater.*, 2009, **21**, 5701–5703.
- 65 W. Huang, Z. Zhu, L. Wang, S. Wang, H. Li, Z. Tao, J. Shi, L. Guan and J. Chen, *Angew. Chem., Int. Ed.*, 2013, **52**, 9162–9166.
- 66 Z. Song, Y. Qian, X. Liu, T. Zhang, Y. Zhu, H. Yu, M. Otani and H. Zhou, *Energy Environ. Sci.*, 2014, **7**, 4077–4086.
- 67 B. Huskinson, M. P. Marshak, C. Suh, S. Er, M. R. Gerhardt, C. J. Galvin, X. Chen, A. Aspuru-Guzik, R. G. Gordon and M. J. Aziz, *Nature*, 2014, **505**, 195–198.
- 68 K. Lin, R. Gómez-Bombarelli, E. S. Beh, L. Tong, Q. Chen, A. Valle, A. Aspuru-Guzik, M. J. Aziz and R. G. Gordon, *Nat. Energy*, 2016, **1**, 16102.
- 69 M. Bahari, Y. Jing, S. Jin, M. Goulet, T. Tsukamoto, R. G. Gordon and M. J. Aziz, *ACS Appl. Mater. Interfaces*, 2024, **16**, 52144–52152.
- 70 C. G. Armstrong and K. E. Toghiani, *Electrochem. Commun.*, 2018, **91**, 19–24.
- 71 Y. Ding, C. Zhang, L. Zhang, Y. Zhou and G. Yu, *Chem*, 2019, **5**, 1964–1987.
- 72 G. Tang, Z. Yang and T. Xu, *Cell Rep. Phys. Sci.*, 2022, **3**, 101195.
- 73 M.-A. Goulet, L. Tong, D. A. Pollack, D. P. Tabor, S. A. Odom, A. Aspuru-Guzik, E. E. Kwan, R. G. Gordon and M. J. Aziz, *J. Am. Chem. Soc.*, 2019, **141**, 8014–8019.
- 74 Y. Jing, E. W. Zhao, M.-A. Goulet, M. Bahari, E. M. Fell, S. Jin, A. Davoodi, E. Jónsson, M. Wu and C. P. Grey, *Nat. Chem.*, 2022, **14**, 1103–1109.
- 75 S. Huang, H. Zhang, M. Salla, J. Zhuang, Y. Zhi, X. Wang and Q. Wang, *Nat. Commun.*, 2022, **13**, 4746.
- 76 M. Chen, R. Chen, I. Zhitomirsky, G. He and K. Shi, *Mater. Sci. Eng., R*, 2024, **161**, 100865.
- 77 L. Xu, Q. Wang, D. Guo, J. Xu, J. Cao, L. Xu, Q. Wang, D. Guo, J. Xu and J. Cao, *New J. Chem.*, 2023, **47**, 11216–11221.
- 78 A. M. Alfaraidi, D. Xi, N. Ni, T. Y. George, T. Tsukamoto, R. G. Gordon, M. J. Aziz and R. Y. Liu, *ACS Appl. Energy Mater.*, 2023, **6**, 12259–12266.



## Review

- 79 B. Hosseinzadeh and M. Ahmadi, *Mater. Today Sustainability*, 2023, **23**, 100468.
- 80 D. G. Kwabi, K. Lin, Y. Ji, E. F. Kerr, M.-A. Goulet, D. De Porcellinis, D. P. Tabor, D. A. Pollack, A. Aspuru-Guzik, R. G. Gordon and M. J. Aziz, *Joule*, 2018, **2**, 1894–1906.
- 81 Y. Ji, M.-A. Goulet, D. A. Pollack, D. G. Kwabi, S. Jin, D. De Porcellinis, E. F. Kerr, R. G. Gordon and M. J. Aziz, *Adv. Energy Mater.*, 2019, **9**, 1900039.
- 82 F. Hasan, V. Mahanta and A. A. A. Abdelazeez, *Adv. Mater. Interfaces*, 2023, **10**, 2300268.
- 83 J. B. Gerken, A. Stamoulis, S.-E. Suh, N. D. Fischer, Y. J. Kim, I. A. Guzei and S. S. Stahl, *Chem. Commun.*, 2020, **56**, 1199–1202.
- 84 Y. Jing, E. M. Fell, M. Wu, S. Jin, Y. Ji, D. A. Pollack, Z. Tang, D. Ding, M. Bahari, M.-A. Goulet, T. Tsukamoto, R. G. Gordon and M. J. Aziz, *ACS Energy Lett.*, 2021, **7**, 226–235.
- 85 C. O. Wilhelmsen, A. Pasadakis-Kavounis, J. V. Christiansen, T. Isbrandt, M. R. Almind, T. O. Larsen, J. Hjelm, J. L. Sørensen and J. Muff, *ACS Sustain. Chem. Eng.*, 2023, **11**, 9206–9215.
- 86 R. B. Jethwa, E. W. Zhao, R. N. Kerber, E. Jónsson, D. S. Wright and C. P. Grey, *J. Mater. Chem. A*, 2021, **9**, 15188–15198.
- 87 M. Wu, Y. Jing, A. A. Wong, E. M. Fell, S. Jin, Z. Tang, R. G. Gordon and M. J. Aziz, *Chem*, 2020, **6**, 1432–1442.
- 88 A. Permatasari, W. Lee and Y. Kwon, *Chem. Eng. J.*, 2020, **383**, 123085.
- 89 A. Alem, P. Poormehrabi, J. Lins, L. Pachernegg-Mair, C. Bandl, V. Ruiz, E. Ventosa, S. Spirk and T. Gutmann, *Energy Environ. Sci.*, 2025, **18**, 7373–7401.
- 90 A. Khetan, *Batteries*, 2023, **9**, 24.
- 91 S. Er, C. Suh, M. P. Marshak and A. Aspuru-Guzik, *Chem. Sci.*, 2015, **6**, 885–893.
- 92 L. Tong, M.-A. Goulet, D. P. Tabor, E. F. Kerr, D. De Porcellinis, E. M. Fell, A. Aspuru-Guzik, R. G. Gordon and M. J. Aziz, *ACS Energy Lett.*, 2019, **4**, 1880–1887.
- 93 C. Wang, Z. Yang, Y. Wang, P. Zhao, W. Yan, G. Zhu, L. Ma, B. Yu, L. Wang, G. Li, J. Liu and Z. Jin, *ACS Energy Lett.*, 2018, **3**, 2404–2409.
- 94 Y. A. Gandomi, D. S. Aaron, J. R. Houser, M. C. Daugherty, J. T. Clement, A. M. Pezeshki, T. Y. Ertugrul, D. P. Moseley and M. M. Mench, *J. Electrochem. Soc.*, 2018, **165**, A970.
- 95 S. V. Modak, W. Shen, S. Singh, D. Herrera, F. Oudeif, B. R. Goldsmith, X. Huan and D. G. Kwabi, *Nat. Commun.*, 2023, **14**, 3602.
- 96 A. M. Fenton, R. K. Jha, B. J. Neyhouse, A. P. Kaur, D. A. Dailey, S. A. Odom and F. R. Brushett, *J. Mater. Chem. A*, 2022, **10**, 17988–17999.
- 97 E. W. Zhao, E. Jónsson, R. B. Jethwa, D. Hey, D. Lyu, A. Brookfield, P. A. A. Klusener, D. Collison and C. P. Grey, *J. Am. Chem. Soc.*, 2021, **143**, 1885–1895.
- 98 M. R. Tuttle, E. M. Brackman, F. Sorourifar, J. Paulson and S. Zhang, *J. Phys. Chem. Lett.*, 2023, **14**, 1318–1325.
- 99 Y. Liu, Z. Wu, P. Zhang, J. Wei, J. Li, H. Wang, S. Wen, J. Liang, Y. Chen, T. Dai, Z. Tie, J. Ma, X. Wang and Z. Jin, *Nat. Commun.*, 2025, **16**, 2965.

